nature human behaviour

Article

https://doi.org/10.1038/s41562-023-01714-6

Pain-preferential thalamocortical neural dynamics across species

Received: 24 February 2023

Accepted: 1 September 2023

Published online: 09 October 2023

Check for updates

Yiheng Tu[1,2] ✉, Zhenjiang Li[1,2], Libo Zhang[1,2], Huijuan Zhang[1,2], Yanzhi Bi[1,2], Lupeng Yue[1,2] & Li Hu[1,2] ✉

Searching for pain-preferential neural activity is essential for understanding and managing pain. Here, we investigated the preferential role of thalamocortical neural dynamics in encoding pain using human neuroimaging and rat electrophysiology across three studies. In study 1, we found that painful stimuli preferentially activated the medial-dorsal (MD) thalamic nucleus and its functional connectivity with the dorsal anterior cingulate cortex (dACC) and insula in two human functional magnetic resonance imaging (fMRI) datasets (n = 399 and n = 25). In study 2, human fMRI and electroencephalography fusion analyses (n = 220) revealed that pain-preferential MD responses were identified 89–295 ms after painful stimuli. In study 3, rat electrophysiology further showed that painful stimuli preferentially activated MD neurons and MD–ACC connectivity. These converging cross-species findings provided evidence for pain-preferential thalamocortical neural dynamics, which could guide future pain evaluation and management strategies.

Pain is an unpleasant sensory and emotional experience protecting our body from actual or potential damage[1]. Transient nociceptive stimuli elicit robust responses in a wide range of cortical and subcortical brain regions involved in sensory processing, emotion and cognition[2–5], but whether there is a pain-preferential (that is, responding differentially to pain and other sensory modalities) neural pattern has been hotly debated in recent years. The traditional view supports that different senses are processed in anatomically distinct unisensory areas and converge onto higher-order multisensory areas[6]. Emerging studies challenge this view by showing that traditional unisensory areas are instead multisensory[7,8]. Even the visual and auditory cortices—regions thought to be dedicated to sight and hearing—are activated during pain processing[2,9].

To identify pain-preferential brain responses, an earlier study used functional magnetic resonance imaging (fMRI) to compare blood-oxygen-level-dependent (BOLD) brain responses elicited by painful, electrotactile, visual and auditory stimuli, but only found somatosensory-specific (painful and electrotactile), not pain-specific neural activities[9]. Motivated by searching for more discrete and spatially defined pain signals, later studies used a similar experimental design and multivariate pattern analysis (MVPA) to identify pain-preferential neural responses, but findings were scattered[7,10,11]. Recent efforts have been made to control the salience effect of painful stimuli[5] and consider genetic architectures[12] when distinguishing brain responses triggered by pain and other sensory stimuli. Nevertheless, a pain-preferential neural pattern has yet to be identified.

Unlike other sensory modalities, pain is inherently unpleasant by definition, and pain sensation and pain emotion are closely intertwined[13]. It is thus of interest to explore whether pain-preferential neural activities could be identified in specific pain-ascending pathways, especially those associated with emotional processing[14]. As an ascending hub of most sensory signals, the thalamus consists of multiple nuclei, whose connections with different cortical areas may underlie the processing of different modality information. Previous animal studies have identified two distinct thalamocortical pathways for pain processing: the lateral pathway from lateral thalamic nuclei to primary and secondary somatosensory cortices (S1 and S2) for sensory-discriminative processing, and the medial pathway from medial thalamic nuclei to the prefrontal cortex and ACC for affective-motivational processing[14]. However, few studies have specifically investigated the distinct roles of

[1]CAS Key Laboratory of Mental Health, Institute of Psychology, Chinese Academy of Sciences, Beijing, China. [2]Department of Psychology, University of Chinese Academy of Sciences, Beijing, China. ✉e-mail: yihengtu@gmail.com; huli@psych.ac.cn

https://doi.org/10.1038/s41562-023-01714-6

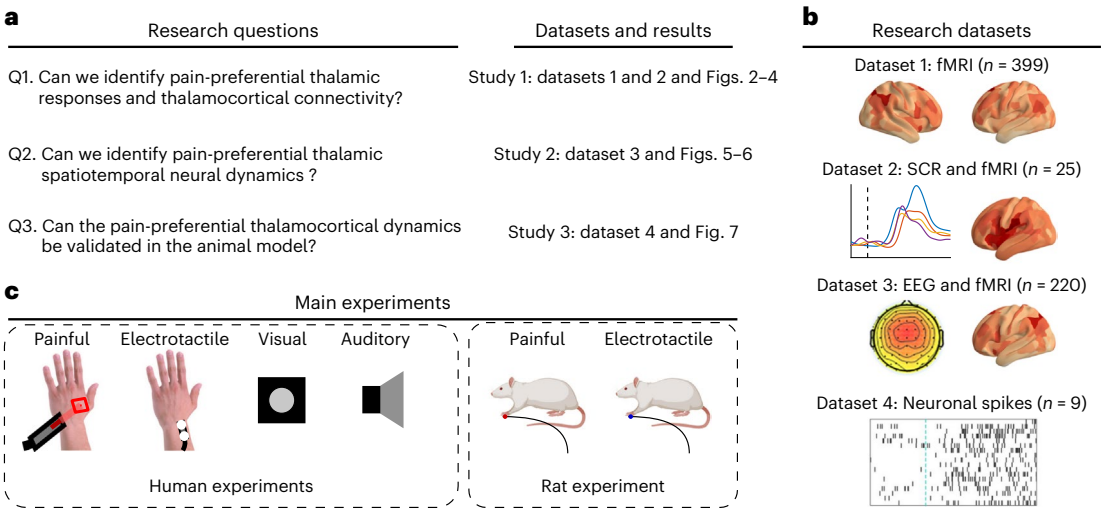

Fig. 1 | Research questions and design. a, This study aims to answer three questions (Q1–3) using three human neuroimaging datasets and a rat electrophysiology dataset. **b**, We acquired fMRI, EEG and SCR data (datasets 1–3) to identify pain-preferential thalamic responses, thalamocortical connectivity and thalamic spatiotemporal neural dynamics (studies 1 and 2). We further validated the pain-preferential thalamocortical dynamics (study 3) in the rat electrophysiology dataset (dataset 4). **c**, In the human experiments (datasets 1–3), participants received four modalities of stimuli: painful, electrotactile, visual and auditory; in the rat experiment, subjects received painful and electrotactile stimuli. This figure was created with BioRender.com.

these two thalamocortical pathways in humans[15], and almost no human study has assessed whether the thalamocortical pathways, especially the medial pathway, are preferentially for pain processing. Moreover, the temporal information (for example, sequential or parallel processing) of thalamocortical neural dynamics in encoding pain is unknown and the clinical translational values of the plausible pain-preferential pathway are unrevealed.

In the present study, we aimed to identify pain-preferential thalamocortical neural dynamics by applying advanced analytic techniques to human neuroimaging and rat electrophysiology datasets (Fig. 1). Specifically, we aimed to address the following three research questions (Fig. 1a): (1) Can we identify pain-preferential thalamic responses and thalamocortical connectivity? (2) Can we identify pain-preferential thalamic spatiotemporal neural dynamics? (3) Can the pain-preferential thalamocortical neural dynamics be validated in directly measured neuronal responses?

To address these questions, we delivered different modalities of sensory stimulation (pain, touch, vision and audition) to a large sample of healthy participants ($n = 399$) and collected their fMRI and electroencephalography (EEG) data. We used these data to identify pain-preferential thalamocortical neural dynamics (studies 1 and 2) based on a machine learning approach (MVPA) and an EEG–fMRI fusion algorithm. In addition, we performed an independent behavioural and fMRI experiment ($n = 25$) with calibrated stimulus intensity to control salience effects on thalamic fMRI responses. Last, we collected rat neuronal spikes when they received painful and electrotactile stimuli. These data enabled us to precisely and directly compare thalamocortical neural dynamics between painful and non-painful somatosensory stimulation (study 3).

Results

Thalamic fMRI responses and thalamocortical connectivity

Simple and isolated sensory stimuli (painful, electrotactile, visual and auditory) of two intensities (high and low) were delivered to 399 healthy participants (Fig. 2a; Methods). Brain responses corresponding to these stimuli were acquired using fMRI in two blocks. We first used general linear modelling (GLM) to identify the brain regions activated by the four modalities of stimuli. Similar to previous studies[7,9], different modalities of sensory stimuli elicited consistent activity in a wide range of brain regions. We observed many spatial overlaps in both cortical and subcortical regions (Fig. 2b). BOLD responses in most of these brain regions were significantly associated with subjective pain reports (Supplementary Fig. 1).

We then parcellated the thalamus into seven distinct nuclei (anterior, pulvinar, medial-dorsal (MD), ventral anterior (VA), ventral latero-ventral (VLV), ventral latero-dorsal (VLD) and central lateral (CL)) in each hemisphere (Fig. 3a) using a probabilistic atlas of the human thalamic atlas[16]. On the basis of the results of GLM analyses, we performed conjunction analyses and found that the posterior part of the ventral lateral thalamus (ventral posterior lateral (VPL)) was preferentially activated by somatosensory stimuli (that is, the cluster was significantly activated by painful and electrotactile stimuli but not by visual and auditory stimuli; $P < 0.001$ at voxel level and $P_{FDR} < 0.05$ at cluster level). The extracted BOLD signals demonstrated significant activation differences in the identified VPL after the onset of stimuli (that is, both painful and electrotactile stimuli significantly more activated the VPL around 4 s than did both visual and auditory stimuli; Fig. 3b). However, we did not observe any significant cluster showing pain-preferential activation on the basis of the GLM results.

Taking advantage of its high sensitivity in detecting differential brain patterns across conditions, we then used MVPA to test the uniqueness of the spatial patterns of thalamic BOLD signals (rather than achieving optimal accuracies using whole-brain voxels) elicited by stimuli in each sensory modality. We constructed support vector machine (SVM)-based binary classifiers to discriminate four modalities of stimuli using the normalized BOLD fMRI signals (to rule out the bulk differences (for example, arousal and attention) in the magnitude of responses to different stimuli) in the thalamus as features (see section on 'MVPA for fMRI'). We used the second volume after each stimulus onset for the MVPA as this volume contained the peak BOLD responses elicited by each stimulus (that is, most likely to contain stimulus-related information). Six binary classifiers were performed: pain (P) versus touch (T), pain (P) versus vision (V), pain (P) versus audition (A), touch (T) versus vision (V), touch (T) versus audition (A) and vision (V) versus audition (A). Figure 3c shows the spatial 'activation patterns' (forward model based on Haufe's method; Methods) that significantly contributed to the discriminations and the classification accuracies for each classifier (*P* versus *T*, 58.3 ± 10.4%; *P* versus *V*, 68.5 ± 11.2%; *P* versus *A*,

https://doi.org/10.1038/s41562-023-01714-6

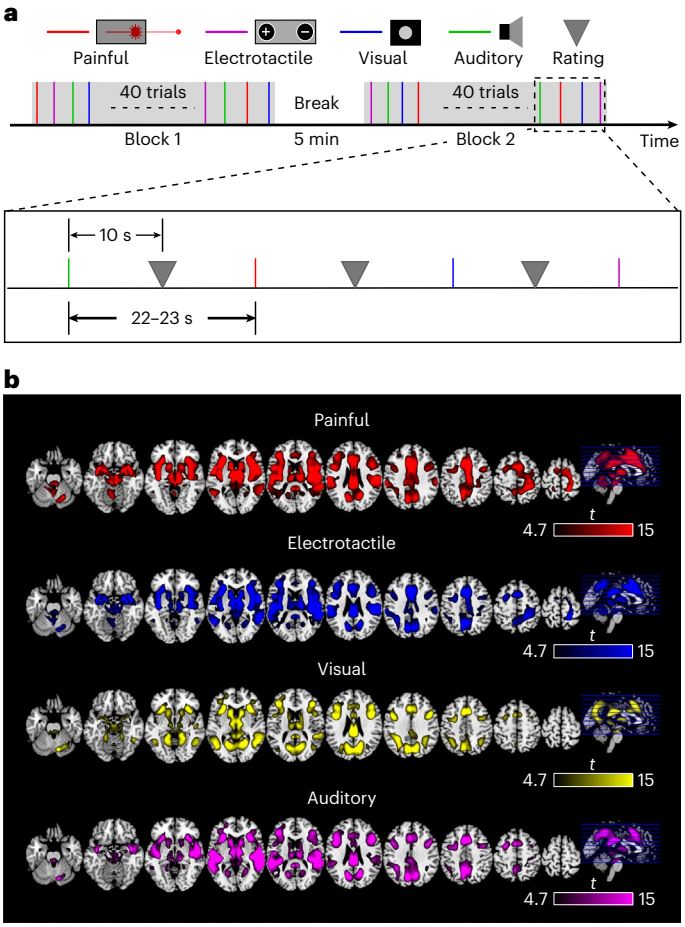

Fig. 2 | Sensory experiment and fMRI BOLD responses. a, Participants (n = 399) received transient stimuli of four sensory modalities (painful, electrotactile, visual and auditory), each comprising two stimuli intensities (high and low). After each stimulus, participants rated their perceived intensity using a numerical rating scale of 0 (no sensation) to 10 (the strongest sensation imaginable). Each participant performed 80 trials (20 for each sensory modality; two blocks) in the MRI scanner. **b**, BOLD responses to painful (red), electrotactile (blue), visual (yellow) and auditory (purple) stimuli. Results were obtained from GLM and thresholded at $P < 0.001$ at the voxel level and $P_{FDR} < 0.05$ at the cluster level.

70.5 ± 10.7%; *T* versus *V*, 66.1 ± 10.7%; *T* versus *A*, 68.4 ± 10.3%). Overall, BOLD signals in the thalamus could significantly distinguish the four modalities of stimuli (the classification accuracies were significantly above 50% in all six classifiers; one-sample *t*-tests against 50%, all $P < 0.001$). We then performed a conjunction analysis across the activation patterns discriminating pain and the other three modalities. We found that BOLD signals in the MD were significantly higher after receiving painful stimuli than electrotactile, visual and auditory stimuli (all $P < 0.001$; Fig. 3d). To minimize the possible influence of differences in subjective pain reports, which are highly associated with stimulus salience, we adopted a within-individual matching procedure to equalize intensity ratings between pain and touch (see section on 'Rating matching procedure' for details of the matching algorithm). After the intensity matching, we found a significant interaction between brain regions (MD versus VPL) and modality (pain versus touch) ($F_{1,165} = 30.08$, $P < 0.001$, $\eta_p^2 = 0.05$). Post hoc tests showed that the MD responses ($T(165) = 3.72$, $P = 0.00027$, Cohen's $d = 0.29$, 95% confidence interval (CI) = (0.017%, 0.057%)) but not the VPL responses ($T(165) = -1.08$, $P = 0.282$, Cohen's $d = 0.08$, 95% CI = (−0.020%, 0.060%)) could significantly discriminate painful and electrotactile stimuli when the intensity ratings were well matched (Supplementary Fig. 2).

After constructing machine learning classifiers to discriminate different sensory modalities, we used the same technique to distinguish two stimulus intensity levels within each modality (for example, high pain versus low pain). We found that BOLD signals in the VPL and MD could discriminate trials following high-pain and low-pain stimuli ($P < 0.001$ at voxel level and $P_{FDR} < 0.05$ at cluster level; 31 voxels and 16 voxels for the right and left clusters, respectively). In contrast, only the VPL could discriminate trials following high electrotactile and low electrotactile stimuli ($P < 0.001$ at voxel level and $P_{FDR} < 0.05$ at cluster level; cluster size, 25 voxels; Fig. 3e). These results in Fig. 3d,e suggest that the MD might be preferentially activated by painful stimuli but not stimuli in other sensory modalities that we investigated, while the VPL was preferentially activated by somatosensory stimuli (for example, both pain and touch).

Since thalamic nuclei have distinct thalamocortical projections, we used psychophysiological interaction (PPI) to evaluate the task-based connectivity between the two identified nuclei patterns; that is, somatosensory-preferential VPL (Fig. 3b) and pain-preferential MD (Fig. 3d) and all other voxels in the brain (see section on 'PPI analysis'). Between-modality comparisons showed increased functional connectivity between the MD and dorsal anterior cingulate cortex (dACC) and bilateral insula (stronger in the anterior part of the insula) after painful stimuli as compared with electrotactile stimuli ($P < 0.001$ at voxel level and $P_{FDR} < 0.05$ at cluster level; Fig. 3f). However, the functional connectivities between the VPL and other brain regions were not significantly different between painful and electrotactile stimuli.

Thalamic fMRI responses after pain–touch salience matching

To address the potential confound of differences in stimulus salience, particularly in thalamic BOLD responses to pain and touch, we conducted an additional independent experiment collecting data from 25 participants, who provided self-reported salience scores and psychophysiological responses (skin conductance response (SCR)), as a recent study suggested that SCR could be an objective measure for salience[17]. The experiment comprised three main sessions (Fig. 4a): (1) a calibration session for familarizing and determining stimulus intensity for painful and electrotactile stimuli; (2) a behavioural session to assess participants' perceived intensity, salience scores and SCR for painful and electrotactile stimuli; and (3) an MRI session to collect BOLD responses following calibrated stimuli with matched salience scores. Detailed information about the experimental procedures can be found in the Methods.

During the behavioural session, participants rated the intensity and salience of painful and electrotactile stimuli, whose physical intensity was calibrated individually from the first session. There were no significant differences between the two modalities in intensity rating ($T(24) = -1.51$, $P = 0.150$, Cohen's $d = 0.30$, 95% CI = (−0.77, 0.22); Fig. 4b), salience rating ($T(24) = -1.91$, $P = 0.068$, Cohen's $d = 0.38$, 95% CI = (−0.76, 0.03); Fig. 4c) and SCR ($T(24) = -0.13$, $P = 0.898$, Cohen's $d = 0.03$, 95% CI = (−0.77, 0.68); Fig. 4d). We observed a significant positive correlation between salience rating and SCR for painful (mean correlation $r = 0.29$, 95% CI = (0.18, 0.40); $T(24) = 5.48$, $P = 1.24 \times 10^{-5}$, one-sample *t*-test against zero) and electrotactile stimuli (mean correlation $r = 0.14$, 95% CI = (0.01, 0.26); $T(24) = 2.31$, $P = 0.030$) within each participant. These results suggest that the calibrated stimuli effectively controlled the salience differences between the two modalities.

During the fMRI session, we selected a subset of stimuli in each participant to match the self-reported salience scores of painful and tactile stimuli. Specifically, for each painful stimulus with salience score of s_p, all tactile trials with the same salience score $s_t = s_p$ were identified and one trial was selected to pair with this particular painful trial. If no tactile stimulus was identified, this painful trial was discarded for further analyses. This method ensured that the selected pairs of painful and electrical stimuli were completely matched on a trial-by-trial level in terms of their salience scores within each participant (mean ± s.d.,

https://doi.org/10.1038/s41562-023-01714-6

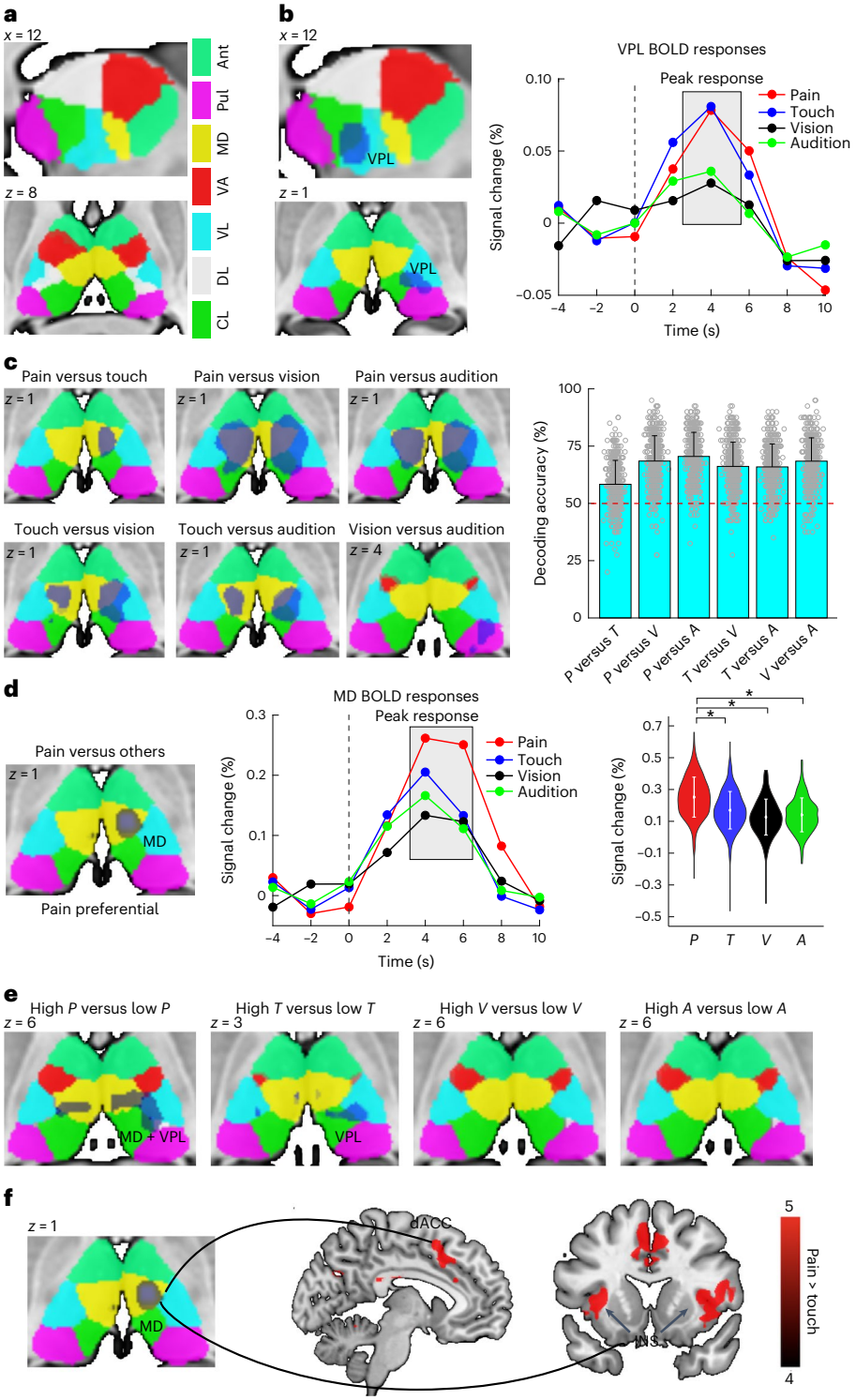

Fig. 3 | Pain-preferential thalamic responses and thalamocortical connectivity. a, The thalamus was parcellated into seven distinct nuclei (anterior (Ant), pulvinar (Pul), MD, VA, VLV, VLD and CL) in each hemisphere using a probabilistic atlas of the human thalamic atlas. **b**, Conjunction analyses based on the GLM activation maps in Fig. 2b showed that the VPL (the shaded area on the thalamic atlas) was preferentially activated by somatosensory stimuli (painful and electrotactile stimuli). **c**, Using MVPA, BOLD signals in the thalamus could significantly distinguish stimuli of the four sensory modalities. The spatial activation patterns (shaded areas on the thalamic atlas) were located in different thalamic nuclei for discriminating between different sensory modalities. **d**, Conjunction analysis based on the spatial activation patterns in Fig. 3c showed that the MD could discriminate between pain and the other three modalities (all $P < 0.001$). **e**, Using MVPA, BOLD signals in the VPL and MD (shaded areas on the thalamic atlas) could discriminate between high and low pain, while only the VPL (shaded area on the thalamic atlas) could discriminate between high and low touch. **f**, Between-modality comparisons showed increased functional connectivity (estimated by PPI) between the MD and dACC and bilateral insula after painful stimuli as compared with electrotactile stimuli. Statistical maps in **b**–**f** were thresholded at $P < 0.001$ at the voxel level and $P_{FDR} < 0.05$ at the cluster level. The bar plots in **c** were compared with the 50% chance level using one-sample *t*-tests and thresholded at $P_{FDR} < 0.05$. The bar plots in **d** were compared across different modalities using paired-sample *t*-tests and thresholded at $P_{FDR} < 0.05$ (indicated by asterisks). Error bars are standard deviations with means as the centre. Results were obtained from 399 participants.

https://doi.org/10.1038/s41562-023-01714-6

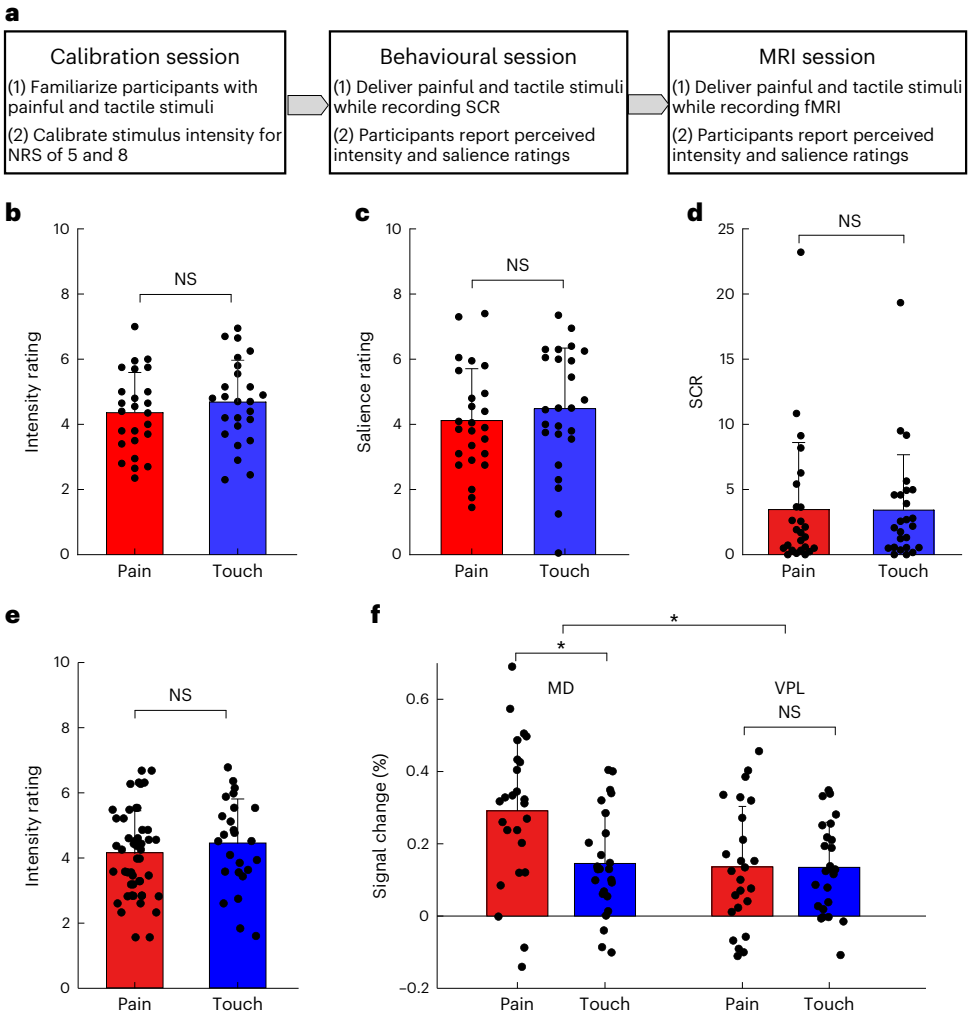

Fig. 4 | The experimental design and results for controlling salience effects on thalamic BOLD responses. a, The experiment comprised three sessions: calibration, behavioural and MRI. **b**,**c**, With the calibrated stimulus intensity, participants reported comparable perceived intensity ($T(24) = -1.51$, $P = 0.150$, Cohen's $d = 0.30$, 95% CI = (−0.77, 0.22)) and salience ratings ($T(24) = -1.91$, $P = 0.068$, Cohen's $d = 0.38$, 95% CI = (−0.76, 0.03)) after painful and electrotactile stimuli in the behavioural session. **d**, Participants had similar levels of SCRs after painful and electrotactile stimuli in the behavioural session ($T(24) = -0.13$, $P = 0.898$, Cohen's $d = 0.03$, 95% CI = (−0.77, 0.68)). **e**, In the fMRI session, after selecting trials with completely matched salience scores, participants had comparable perceived intensity after painful and electrotactile stimuli ($T(24) = 1.90$, $P = 0.070$, Cohen's $d = 0.38$, 95% CI = (−0.03, 0.64)). **f**, In salience-matched trials, MD responses were significantly higher in painful trials than in electrotactile trials ($T(24) = 3.02$, $P = 0.006$, Cohen's $d = 0.60$, 95% CI = (0.05%, 0.25%)), while VPL responses did not differ significantly between painful and electrotactile stimuli ($T(24) = 0.03$, $P = 0.976$, Cohen's $d = 0.006$, 95% CI = (−0.08%, 0.08%)). Error bars represent standard deviations. Results were obtained from 25 participants. Paired-sample *t*-tests and two-way repeated-measures ANOVA tests were used for data analyses (followed by post hoc comparisons using Bonferroni-corrected two-sided paired-sample *t*-tests). NS, not significant ($P > 0.05$); *, $P < 0.05$.

4.14 ± 1.52). Moreover, the perceived intensities of painful and tactile trials were also not significantly different (painful, 4.15 ± 1.32; tactile, 4.45 ± 1.38; $T(24) = 1.90$, $P = 0.070$, Cohen's $d = 0.38$, 95% CI = (−0.03, 0.64); Fig. 4e).

We then extracted BOLD fMRI signals (the second volume after each stimulus onset) in the MD and VPL and compared the responses between painful and electrotactile trials using two-way repeated-measures analysis of variance (ANOVA). The results (Fig. 4f) showed a significant main effect of the two nuclei ($F_{1,24} = 28.01$, $P = 1.99 \times 10^{-5}$, $\eta_p^2 = 0.54$) and a significant interaction effect of nuclei and modalities ($F_{1,24} = 48.42$, $P = 3.40 \times 10^{-7}$, $\eta_p^2 = 0.67$). Post hoc analyses showed that MD responses were significantly higher in painful trials compared to electrotactile trials ($T(24) = 3.02$, $P = 0.006$, Cohen's $d = 0.60$, 95% CI = (0.05%, 0.25%)), but VPL responses were not ($T(24) = 0.03$, $P = 0.976$, Cohen's $d = 0.006$, 95% CI = (−0.08%, 0.08%)).

To externally validate our findings, we gathered and re-analysed data ($n = 51$) from a published study[5] where the perceived intensity of painful and electrotactile stimuli was matched on the basis of individually calibrated stimulus intensity. Further details regarding the experimental design and data collection can be found in Supplementary Fig. 3. Using this dataset, we found that the MD responses were significantly higher after painful stimuli than electrotactile stimuli ($T(50) = 2.61$, $P = 0.012$, Cohen's $d = 0.37$, 95% CI = (0.02%, 0.17%); Supplementary Fig. 3), while VPL responses were not significantly different between painful and electrotactile trials ($T(50) = 0.26$, $P = 0.796$, Cohen's $d = 0.04$, 95% CI = (−0.069%, 0.089%)).

EEG responses and EEG–fMRI fusion responses

We located the MD as a pain-preferential thalamic nucleus in the fMRI analyses. However, due to the low temporal resolution of fMRI, we were unaware of when this nucleus processed pain-preferential

https://doi.org/10.1038/s41562-023-01714-6

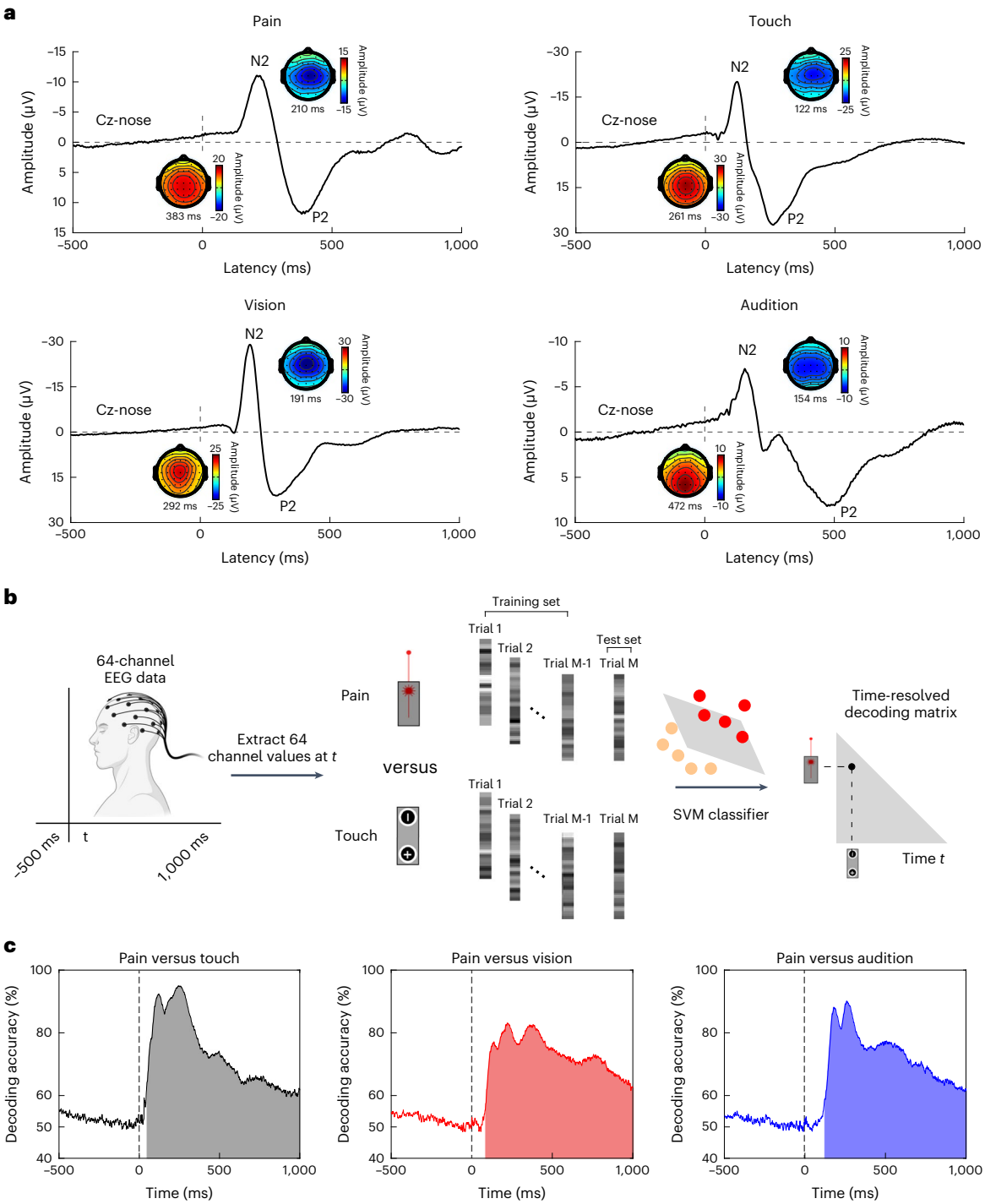

Fig. 5 | EEG time series and decoding performance. a, Sensory stimuli of four modalities (painful, electrotactile, visual and auditory) elicited clear EEG responses. **b**, For each time point in the peristimulus EEG signal, from −500 to 1,000 ms (1 ms resolution) with respect to stimulus onset, pattern vectors were constructed by concatenating the 64 EEG electrode measures into 64-dimensional vectors as features. Time-resolved MVPA was performed to classify pairwise between different stimulus modalities. The resultant classification accuracies were stored in a symmetric 4 × 4 decoding matrix per time point and participant. **c**, The time courses of neural decoding accuracy for distinguishing pain and the other three modalities. EEG signals could significantly discriminate pain and the other three modalities before 100 ms and remained significantly above chance at 1,000 ms after stimulus onset (cluster-corrected sign-permutation test; cluster-defining threshold $P < 0.001$, cluster-corrected significance level $P < 0.05$). Results were obtained from 220 participants. This figure was created with BioRender.com.

information to discriminate between pain and the other three modalities. To address this issue, we collected EEG data from 220 participants who also finished the fMRI experiment. Experimental details in the EEG dataset were almost identical to the fMRI dataset, except that the timings were adapted. Healthy participants received different modalities of sensory stimuli (painful, electrotactile, visual and auditory) and of two intensities (high and low), and rated their subjective perception using the numerical rating scale (NRS). We observed clear stimulus-evoked EEG responses for all sensory modalities (Fig. 5a).

https://doi.org/10.1038/s41562-023-01714-6

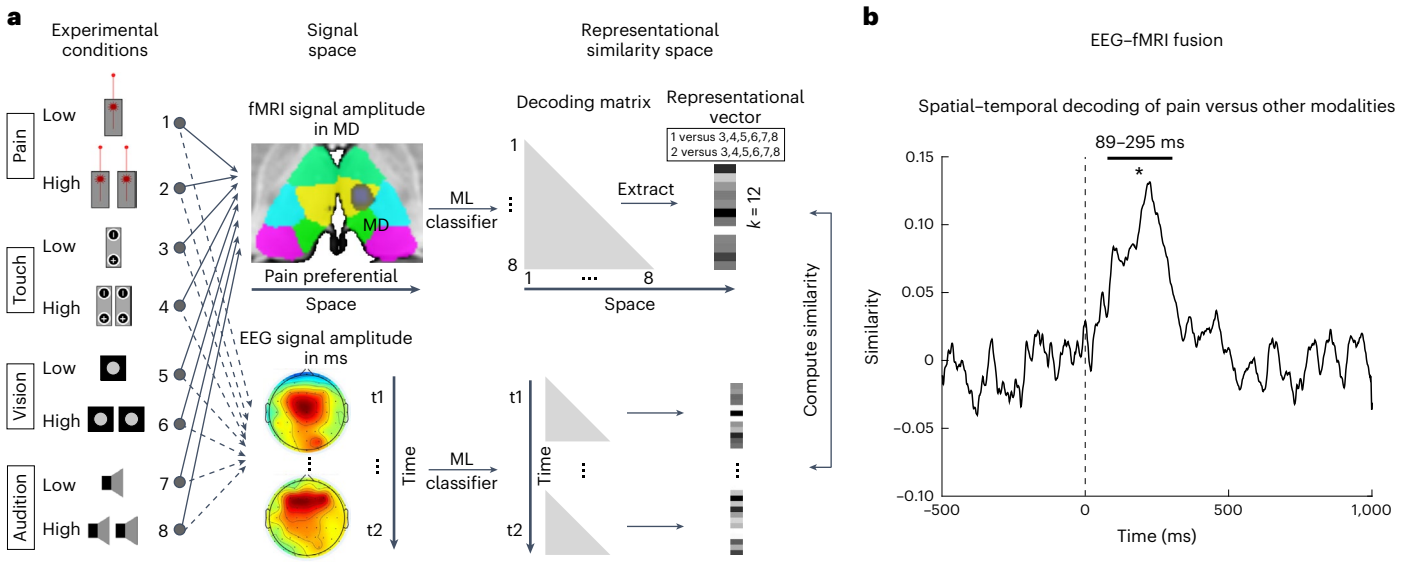

Fig. 6 | EEG–fMRI fusion decoding performance. a, A decoding vector including 12 binary tasks to discriminate pain and the other three modalities (high/low pain versus high/low touch/vision/audition, at within-participant level) was constructed. For fMRI, we used voxel-wise BOLD signals in the MD as features for these 12 classification tasks, resulting in a vector of classification accuracies (fMRI dissimilarity vector) for each participant. For EEG, we used 64-channel EEG data at each time point as features for these 12 classification tasks, resulting in a vector of classification accuracies (EEG dissimilarity vector) for each time point and each participant. The extent of representational similarity between participant-level fMRI in the MD and EEG was evaluated by computing Spearman's rank-order correlations between the fMRI dissimilarity vector and EEG dissimilarity vectors (separately for each time point). **b**, Averaged time-resolved similarity indices (across 220 participants) showed that fMRI BOLD responses in the MD and EEG responses were significantly correlated within the time interval ranging from 89 to 295 ms when distinguishing pain and other three modalities (sign-permutation test, cluster-defining threshold $P < 0.001$, cluster-corrected significance level $P < 0.05$). Results were obtained from 220 participants. *, $P < 0.05$.

We then tested whether the scalp EEG could discriminate between pain and the other three modalities. For each time point in the peri-stimulus EEG signal, from −500 to 1,000 ms (1 ms resolution) with respect to stimulus onset, we constructed pattern vectors by concatenating the 64 EEG electrode measures into 64-dimensional vectors as features. We performed time-resolved MVPA (with cross-validation) to classify pairwise between different sensory modalities (Fig. 5b). The resultant classification accuracies were stored in a symmetric 4 × 4 decoding matrix (each cell indicated the accuracy that the classifier distinguished between two modalities) per time point and participant. Figure 5c shows the time courses of neural decoding accuracy for distinguishing pain and the other three modalities by averaging the cells in the decoding matrix across participants. We found that EEG signals could significantly discriminate pain and other three modalities before 100 ms (decoding first reaches significance, pain versus touch 27 ms; pain versus vision 76 ms; pain versus audition 97 ms) and remained significantly above chance until >1,000 ms after stimulus onset (cluster-corrected sign-permutation test; cluster-defining threshold $P < 0.001$, cluster-corrected significance level $P < 0.05$). Direct comparisons of the decoding time courses showed that distinguishing pain and touch was earlier than (1) distinguishing pain and vision ($P < 0.001$, bootstrap testing) and (2) distinguishing pain and audition ($P < 0.001$, bootstrap testing).

Since both fMRI signals in the MD and scalp EEG responses could discriminate pain and the other three modalities, we then examined if they were associated and could represent distinct thalamocortical neural dynamics during a particular time window when the pain was experienced. Leveraging the data from these participants ($n = 220$) who performed both fMRI and EEG experiments, we used the EEG–fMRI fusion technique (see section on 'EEG–fMRI fusion analysis') to investigate when representations extracted from EEG were correlated with those extracted from fMRI in the MD. This computational approach enabled us to resolve human brain responses in space and time based on the suggestion that the thalamocortical neural dynamics are measured in particular locations at particular time points[18].

In brief (Fig. 6a), we built a decoding vector including 12 binary tasks to discriminate pain and the other three modalities (high/low pain versus high/low touch/vision/audition, at within-participant level). For fMRI, we used voxel-wise BOLD signals (the second volume after each stimulus) in the MD as features for these 12 classification tasks, resulting in a vector of classification accuracies (fMRI dissimilarity vector) for each participant. For EEG, we used 64-channel EEG data at each time point as features for these 12 classification tasks, resulting in a vector of classification accuracies (EEG dissimilarity vector) for each time point and each participant. We then evaluated the extent of representational similarity between participant-level fMRI in the MD and EEG by computing Spearman's rank-order correlations between fMRI dissimilarity vector and EEG dissimilarity vectors (separately for each time point) (Fig. 6b). As a result, we were able to obtain time-resolved similarity indices for each participant and perform statistical analyses across 220 participants to identify the time window in which fMRI BOLD responses in the MD and EEG signals were significantly correlated when distinguishing pain and the other three modalities. We found that EEG dissimilarity vectors correlated with fMRI dissimilarity vectors in the MD between 89 and 295 ms (peaked at 223 ms; sign-permutation test, cluster-defining threshold $P < 0.001$, cluster-corrected significance level $P < 0.05$), which provided time stamps for MD-based thalamocortical neural dynamics during pain processing. We also performed the same analysis using the voxel-wise BOLD signals in the VPL as features. The fMRI BOLD responses in the VPL and EEG signals were significantly correlated earlier; that is, between 65 and 159 ms (Supplementary Fig. 4). These results showed distinct temporal characteristics in the two ascending pathways; that is, starting earlier in processing sensory-discriminative information in the lateral pain pathway and later in delivering the valence-coded emotional information in the medial pain pathway.

Pain-preferential thalamic neural dynamics in rats

To further validate the pain-preferential thalamocortical dynamics, we collected the neuronal spike activity of rats when they received painful and electrotactile stimuli ($n = 9$; Fig. 7a,b). In Fig. 7c, all brain regions showed strong stimulus-evoked neuronal responses after painful stimuli. Two-way repeated-measures ANOVA revealed a significant main effect of stimulus intensity ($F_{1,8} = 9.56$, $P = 0.014$, $\eta_p^2 = 0.54$). Post hoc paired-sample t-tests suggested that all brain areas were modulated by stimulus intensity (VPL: $T(8) = 2.63$, $P = 0.034$, Cohen's $d = 2.54$, 95% CI = (1.25, 25.18); S1: $T(8) = 3.60$, $P = 0.007$, Cohen's $d = 3.59$, 95% CI = (5.64, 25.90); MD: $T(8) = 2.89$, $P = 0.025$, Cohen's $d = 2.72$, 95% CI = (2.21, 26.37); ACC: $T(8) = 2.63$, $P = 0.030$, Cohen's $d = 2.62$, 95% CI = (2.26, 35.14)). In Fig. 7d, VPL showed the strongest stimulus-evoked neuronal responses after tactile stimuli. Two-way repeated-measures ANOVA demonstrated a significant interaction between stimulus intensity and brain area ($F_{3,24} = 4.23$, $P = 0.015$, $\eta_p^2 = 0.34$). Post hoc paired-sample t-tests suggested that high-intensity stimuli induced significantly stronger neuronal responses than low-intensity stimuli in the VPL ($T(8) = 2.32$, $P = 0.049$, Cohen's $d = 2.31$, 95% CI = (0.03, 28.93)) but not in other brain regions (S1: $T(8) = 1.01$, $P = 0.34$, Cohen's $d = 1.01$, 95% CI = (−8.99, 3.50); MD: $T(8) = 0.44$, $P = 0.67$, Cohen's $d = 0.43$, 95% CI = (−7.09, 4.83); ACC: $T(8) = 1.74$, $P = 0.12$, Cohen's $d = 1.72$, 95% CI = (−15.29, 2.21)). These neuronal spike activities directly showed that painful but not electrotactile stimuli preferentially elicited neuronal responses in the MD.

Spike–spike coherence (SSC) between pairs of brain regions showed different pathway patterns between painful and electrotactile modalities. Whereas clear SSC was observed in both VPL–S1 and MD–ACC pathways for painful stimuli (0–200 ms, 1–40 Hz), evident SSC was only observed in the VPL–S1 pathway for electrotactile stimuli (0–100 ms, 1–40 Hz). In Fig. 7e, two-way repeated-measures ANOVA showed a significant main effect of stimulus intensity ($F_{1,8} = 18.76$, $P = 0.002$, $\eta_p^2 = 0.70$) and pathway ($F_{1,8} = 21.24$, $P = 0.001$, $\eta_p^2 = 0.72$) for painful stimuli. Post hoc paired-sample t-tests suggested that high-intensity stimuli induced significantly stronger SSC than low-intensity stimuli in both pathways (VPL–S1: $T(8) = 2.90$, $P = 0.021$, Cohen's $d = 2.85$, 95% CI = (0.004, 0.035); MD–ACC: $T(8) = 4.20$, $P = 0.003$, Cohen's $d = 4.01$, 95% CI = (0.017, 0.064)). Meanwhile, the MD–ACC pathway had significantly stronger SSC than the VPL–S1 pathway in both stimulus intensities (low intensity: $T(8) = 3.36$, $P = 0.015$, Cohen's $d = 3.05$, 95% CI = (0.01, 0.073); high intensity: $T(8) = 5.81$, $P = 0.0004$, Cohen's $d = 5.67$, 95% CI = (0.037, 0.088)). In Fig. 7f, two-way repeated-measures ANOVA showed a significant main effect of the pathway for electrotactile stimuli ($F_{1,8} = 83.57$, $P = 1.65 \times 10^{-5}$, $\eta_p^2 = 0.91$). Post hoc paired-sample t-tests suggested that the VPL–S1 pathway had significantly stronger SSC than the MD–ACC pathway in both stimulus intensities (low intensity: $T(8) = 7.64$, $P = 6.04 \times 10^{-5}$, Cohen's $d = 7.64$, 95% CI = (0.072, 0.134); high intensity: $T(8) = 7.68$, $P = 2.10 \times 10^{-5}$, Cohen's $d = 8.84$, 95% CI = (0.092, 0.156)).

Discussion

In this study, we identified and validated pain-preferential thalamocortical neural dynamics across species. Applying MVPA decoding and PPI analysis to fMRI datasets ($n = 399$ and 25), we found that MD BOLD responses and MD–dACC/insula functional connectivity were preferentially activated by painful stimuli (Fig. 3) and the pain-preferential thalamic fMRI responses were not confounded by stimulus salience (Fig. 4). Moving beyond the traditional fMRI studies, we applied a data fusion technique to a unique EEG–fMRI dataset ($n = 220$), which enabled us to temporally identify pain-preferential brain responses in the MD from 89 to 295 ms (Figs. 5 and 6). By placing electrodes in thalamic nuclei (MD and VPL) and cortical regions (ACC and S1), we validated that the MD and MD–ACC connectivity were also preferentially activated by painful stimuli in rats (Fig. 7).

Searching for pain-preferential neural activity using neuroimaging techniques has been a challenging but meaningful task for both understanding and controlling pain[19]. In the last two decades, many studies have aimed at understanding how cortical and subcortical structures process nociceptive stimuli and how pain perception emerges from these neural processes in the human brain[2,3,20,21]. These studies have found a wide range of brain regions (for example, the S1, S2, cingulate cortex, insula and thalamus) that respond to painful stimuli and correlate with the perceived intensity of pain. The brain activity in these regions could constitute a 'signature' of the neural processes underlying pain and pain modulation[2], and is claimed to serve as an objective measure for the experience of pain. However, the specificity of the pain 'signature' has been challenged since the brain activities in these regions are also influenced by factors other than pain perception, such as stimulus salience[4,22] and cognitive control[23,24]. For instance, most brain responses evoked by painful stimuli can also be activated by equally salient but non-painful electrotactile, auditory and visual stimuli[7,9] (see also Fig. 2b), even in patients with congenital pain insensitivity[25]. Therefore, even though the pain signature is strongly associated with pain, it could not be pain preferential.

Although almost all intense transient sensory stimuli are intrinsically salient (stand out relative to other environmental stimuli), pain is inherently unpleasant by definition[13]. This unique property of pain suggests that pain-preferential activity may be identified in the medial pain pathway responsible for pain affective processing. Specifically, the MD-relayed medial pathway, not the VPL-relayed lateral pathway, may contain pain-preferential thalamocortical neural dynamics. This suggestion was confirmed by converging evidence in the present study, in which we directly targeted the spinothalamic tracts in healthy individuals (Figs. 3–6) and rats (Fig. 7). Notably, our results that pain-preferential activity could be identified in the MD-relayed medial pain pathway (between the MD and dACC/insula) also agree with previous human fMRI studies showing that the opercula-insular and cingulate cortices play a crucial role in pain processing[26,27]. One may argue that the dACC and insula do not preferentially respond to pain, since these brain areas are also involved in capturing attention to detect salient stimuli from the noise environment[28]. However, this salience perspective could not provide a sound explanation for our findings, since intense electrotactile, auditory and visual stimuli can be as salient as painful stimuli (especially when intensity ratings were well matched between modalities; Supplementary Figs. 2 and 3), but activation patterns in the MD and MD–dACC/insula connectivity can distinguish between painful stimuli and other non-painful stimuli. More importantly, we also showed that the MD but not VPL BOLD responses could discriminate painful and electrotactile stimuli when the salience levels of stimuli were comparable (Fig. 4).

To offer cross-species and multilevel (macrolevel and mesolevel) insights into the pain-preferential encoding of pain information in the MD-relayed ascending pathway, we also validated our findings from human participants with rodents. On the basis of an experimental design similar to human studies, we confirmed that the MD and MD–dACC connectivity were preferentially activated by painful stimuli in rats (Fig. 7). Painful stimuli induced significant MD neuronal responses and MD–ACC connectivity but these neural dynamics were not observed following electrotactile stimuli. In contrast, VPL neuronal responses and VPL–S1 connectivity were elicited by both painful and electrotactile stimuli. Interestingly, similar to fMRI results, the VPL could discriminate between high and low intensities of painful and electrotactile stimuli, while the MD could only discriminate between high and low painful stimuli, not electrotactile stimuli. Although direct cross-species comparisons are difficult, the finding that pain-preferential thalamocortical dynamics (neuronal responses in the thalamus and its targeted cortex) in rats occurred around 100 ms after stimulus onset (Fig. 7c) were consistent with our findings from EEG–fMRI fusion analysis (Fig. 6b). Since fMRI is not a direct measure of neuronal activity[29], our results from rat neuronal spikes provided direct evidence of the pain-preferential thalamocortical dynamics in the MD.

https://doi.org/10.1038/s41562-023-01714-6

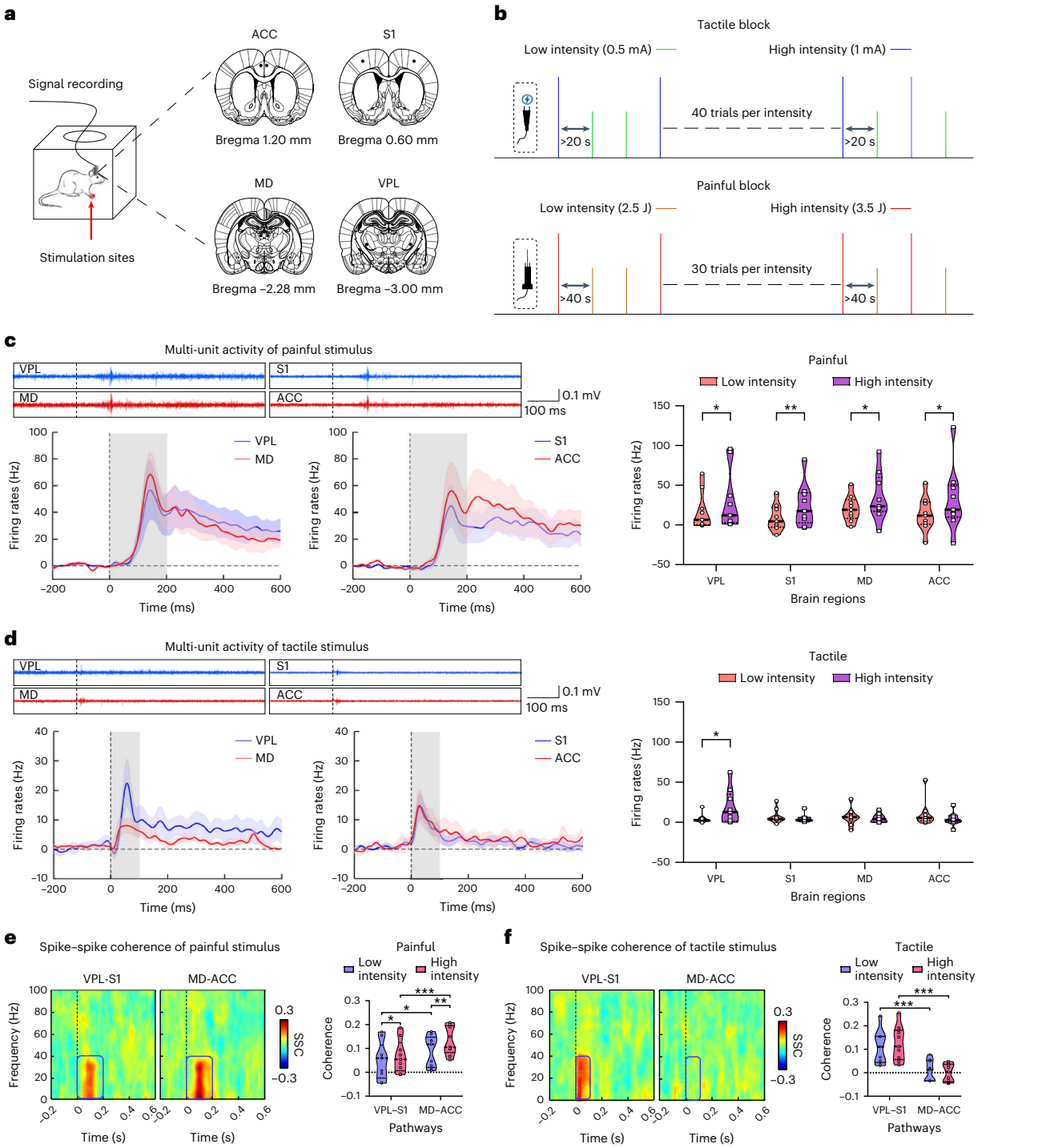

Fig. 7 | Experiment and spike results in rats. a, Rats ($n = 9$) were permitted to move freely in a plastic chamber. Stimuli were delivered to the plantar surface of either the left or right forepaw. The neuronal activities of bilateral ACC, S1, MD and VPL of rats were simultaneously recorded. The rat brain slice images are adapted from the rat brain atlas[36]. **b**, Two intensities of painful and electrotactile stimuli were delivered to rats in two separate blocks. **c**, For painful stimuli, the VPL and MD, as well as S1 and ACC, showed comparable neuronal responses within 200 ms. All brain areas were significantly modulated by stimulus intensity ($F_{1,8} = 9.56$, $P = 0.014$; VPL: $T(8) = 2.63$, $P = 0.034$, 95% CI = (1.25, 25.18); S1: $T(8) = 3.60$, $P = 0.007$, 95% CI = (5.64, 25.90); MD: $T(8) = 2.89$, $P = 0.025$, 95% CI = (2.21, 26.37); ACC: $T(8) = 2.63$, $P = 0.030$, 95% CI = (2.26, 35.14)). **d**, For electrotactile stimuli, VPL showed the strongest neuronal responses within 100 ms. Neuronal responses evoked by high-intensity tactile stimuli were significantly higher than low intensity in the VPL ($F_{3,24} = 4.23$, $P = 0.015$; $T(8) = 2.32$, $P = 0.049$, 95% CI = (0.03, 28.93)). **e**, For painful stimuli, strong SSCs were observed between VPL and S1 and between MD and ACC (0–200 ms, 1–40 Hz). High-intensity stimuli induced significantly stronger SSC than low-intensity stimuli for both pathways ($F_{1,8} = 21.24$, $P = 0.001$; VPL–S1: $T(8) = 2.90$, $P = 0.021$, 95% CI = (0.004, 0.035); MD–ACC: $T(8) = 4.20$, $P = 0.003$, 95% CI = (0.017, 0.064)). MD–ACC had significantly stronger SSC than VPL–S1 in both intensities (low intensity: $T(8) = 3.36$, $P = 0.015$, 95% CI = (0.01, 0.073); high intensity: $T(8) = 5.81$, $P = 0.0004$, 95% CI (0.037, 0.088)). **f**, For electrotactile stimuli, strong SSC was also observed between VPL and S1 (0–100 ms, 1–40 Hz) but not between MD and ACC. VPL–S1 had significantly stronger SSC than MD–ACC in both intensities ($F_{1,8} = 83.57$, $P = 1.65 \times 10^{-5}$; low intensity: $T(8) = 7.64$, $P = 6.04 \times 10^{-5}$, 95% CI = (0.072, 0.134); high intensity: $T(8) = 7.68$, $P = 2.10 \times 10^{-5}$, 95% CI = (0.092, 0.156)). Two-way repeated-measures ANOVA tests were used for all data analyses, followed by post hoc comparisons using Bonferroni-corrected two-sided paired t-tests. *, $P < 0.05$; **, $P < 0.01$.

Understanding the thalamocortical neural dynamics in humans may have the potential to impact the clinical evaluation and management of pain. A recent study indicated that functional abnormalities in the MD and MD–insula connectivity were associated with the pathophysiology of chronic low back pain[30]. Our present study demonstrated that the MD-based neural dynamics could be pain-preferential: MD responded differently to pain and other sensory modalities, encoding information preferentially associated with pain. Thus, the MD-based neural dynamics could serve as a possible neural marker for evaluating acute and chronic pain, offering a means to focus on pain-related information while minimizing irrelevant or confounding factors. This is particularly relevant in patients with altered pain sensitivity but intact other sensory functions, such as those with neuropathic pain who may exhibit pain hypersensitivity[31,32] or people with schizophrenia who may have pain hyposensitivity[33]. In addition, the pain-preferential neural dynamics have the potential to identify targets for non-pharmacological interventions, for example, brain stimulation therapies. Apart from invasively stimulating brain regions using deep brain stimulation, recent advances in non-invasive deep brain stimulation, such as temporal interference stimulation[34] and focused ultrasound stimulation[35], hold promise for targeting the MD-based neural dynamics to relieve pain. In other words, these innovative approaches may provide opportunities for developing effective interventions by modulating the activity of the MD-based neural dynamics.

There are several limitations in the study. First, we suggest that the pain-preferential encoding in MD is related to the inherent unpleasantness of pain, but this emotion proposal needs direct testing. Although non-nociceptive tactile, auditory and visual stimuli are not necessarily valenced, some forms of these stimuli can be unpleasant, for example, certain affective pictures or grima, the sound of nails scratching a blackboard. These stimuli can serve as controls when testing the emotion proposal. Second, we only considered thalamocortical dynamics following transient laser stimuli. Pain can be induced by various methods such as mechanical pressure, contact heat, cold, ischaemia, electrical and chemical stimuli. Some of them can lead to sustained or tonic pain perception, which is clinically more relevant and more closely related to emotion than is transient pain. Future studies thus need to test whether our findings on MD and MD–ACC connectivity can be generalized to other pain models, especially tonic pain models. Third, it is still of interest to directly examine if there is any impairment of thalamocortical dynamics in those with chronic pain. Some studies have suggested altered thalamocortical connectivity in people with chronic pain[30], but systematic research on this topic is still scarce. In addition to those with chronic pain, further studies can also systematically investigate whether people with specific pain insensitivity also exhibit abnormal MD activity or MD–ACC connectivity. Fourth, our study was correlational. We have shown that MD-based neural dynamics is pain-preferential, but the causal role of MD in pain encoding cannot be determined without further interventional studies. Revealing the causal relationship between MD-based neural dynamics is important not only for a deeper understanding of pain information encoding but also for effective treatment of pain.

Methods

Studies 1 and 2 were approved by the Ethical Committee at the Institute of Psychology, Chinese Academy of Sciences (reference no. H17025). All surgical and experimental procedures in study 3 adhered to the guidelines for animal experimentation by the Animal Care and Use Committee and were approved by the Ethical Committee of the Institute of Psychology, Chinese Academy of Sciences (reference no. H22033).

Overview

This article included three studies with four locally collected independent datasets (three neuroimaging datasets and one rat electrophysiology dataset; not preregistered). The first three datasets included fMRI (dataset 1, $n = 399$; dataset 2, $n = 25$) and EEG data (dataset 3, n = 220; these participants also finished fMRI experiments) from healthy participants who were experiencing different modalities of sensory stimulation. Given the large sample size and a well-validated experimental design, the data had sufficient power to identify pain-preferential thalamic responses and thalamocortical connectivity (study 1). Moreover, taking advantage of the unique EEG–fMRI data (participants who finished the same experiment and sampled by EEG and fMRI separately) and the state-of-the-art data fusion technique, we were able to characterize thalamocortical neural dynamics in space and time with high resolution (study 2). Dataset 4 included rat electrophysiology data ($n = 9$) where they received painful and tactile stimuli. This dataset enabled us to precisely locate and validate the pain-preferential thalamocortical dynamics (study 3).

Human participants

Study 1 included 399 healthy participants from dataset 1 (160 males; age 21.3 ± 3.8 yr, mean ± s.d.; two participants did not provide demographic information) and 25 healthy participants from dataset 2 (3 males; age 22.3 ± 2.9 yr) who were pain-free and had no history of chronic pain and neuropsychiatric disorders. Study 2 included 220 healthy participants (92 males; age 20.8 ± 2.3 yr) who also participated in study 1 (dataset 1). All participants in studies 1 and 2 gave written consent forms. Participants were compensated monetarily for their participation in studies 1 and 2.

Rats

Study 3 used nine adult male Sprague Dawley rats (weighing 350–450 g). Rats were housed in separate cages and were free to obtain water and food under controlled conditions of room temperature at 23 °C, air humidity of 60% and a 12 h dark–light cycle.

Data acquisition

In studies 1 and 2, we acquired task-based fMRI and structural MRI scans using 3.0 Tesla MRI system with the standard 64-channel head coil (Discovery MR 750, General Electric Healthcare). Details of the MRI acquisition parameters for datasets 1 and 2 can be found in Supplementary Table 1.

In study 2, we acquired task-based EEG data via 64 AgCl electrodes positioned according to the International 10–20 System, using the nose as reference (band-pass filter, 0.01–100 Hz; sampling rate, 1,000 Hz; Brain Products EEG system). Electrode impedance was kept <10 kΩ. Electro-oculographic signals were simultaneously recorded using two surface electrodes, one placed ~10 mm below the left eye and the other placed ~10 mm from the outer canthus of the left eye.

In study 3, we acquired the rat electrophysiological data using a 32-channel OmniPlex system (sampling rate 40 kHz, Plexon). The implantation coordinates of each brain region were selected according to the rat brain atlas[36]. For simultaneous bilateral ACC (AP, +1.2 mm; ML, ±0.6 mm; DV, −1.2 mm from the brain surface, the same below), S1 (AP, +0.6 mm; ML, ±3.2 mm; DV, −1.5 mm), MD (AP, −2.3 mm; ML, ±0.8 mm; DV, −5.0 mm) and VPL (AP, −3.0 mm; ML, ±3.0 mm; DV, −6.0 mm) recordings, eight tetrodes of tungsten wires array (20 μm in diameter, California Fine Wires Company) were implanted for recording multi-unit activity (MUA). The impedance of each tetrode was between 2 and 2.5 MΩ. Two epidural electrodes made of stainless steel screws (diameter, 1 mm) were set as reference and ground, which were placed on the middle line, 2 and 4 mm caudally to the lambda[37], respectively. To confirm the microelectrode tip location in the brain tissue section, all electrodes were immersed in cell red fluorescent dye DiI solution (Yeasen Biotechnology) before surgical implantation (Supplementary Fig. 5).

Data preprocessing

fMRI data preprocessing. The fMRI data were preprocessed and analysed in MATLAB (R2020a; Mathwork) using SPM12 (Wellcome

Trust Center for Neuroimaging). The first five volumes were discarded to allow time for signal equilibration. Images were corrected for slice-timing and head motion. The resulting images were normalized to the Montreal Neurological Institute space[38], spatially smoothed using a Gaussian kernel of 3 mm full width at half maximum and temporally filtered using a band-pass filter (0.01–0.10 Hz). To minimize the effect of head motion on the estimation of thalamic responses and thalamocortical connectivity, we followed the strategy suggested by a benchmark study[39] by combining the six motion estimates and two physiological time series (cerebrospinal fluid and the white matter signals) with global signal regression.

EEG data preprocessing. The EEG data were preprocessed in MATLAB using the EEGLAB toolbox[40]. Continuous EEG data were band-pass filtered between 1 and 30 Hz and were segmented into epochs extending from 500 ms before stimulus onset to 1,000 ms afterwards. Each epoch was baseline corrected using the prestimulus interval. Trials contaminated by eye blinks and movements were corrected using an independent component analysis algorithm ('runica') implemented in the EEGLAB toolbox.

Rat neurophysiological data preprocessing. The rat neurophysiological data were preprocessed using NDManager[41]. Raw data were high-pass filtered at 300 Hz and thresholded at 3 s.d. above the baseline mean to find time intervals containing spiking events. Then, the waveforms of these time intervals were decomposed using a principal component analysis. Furthermore, the spike activity was sorted and grouped into clusters using KlustaKwik[42] and manually screened using klusters[41].

Study 1.1 pain-preferential thalamic responses

Experimental procedures. Participants received transient sensory stimulation, including painful, electrotactile, visual and auditory stimuli. Two stimulus intensities (high and low) were delivered for each sensory modality. The fMRI experiment consisted of two blocks, each with 40 sensory stimuli (5 stimuli for each modality and intensity) delivered in the MRI scanner. After each block, participants were allowed to take a brief rest. The order of stimulus modality and intensity was pseudorandomized in each block. Each trial began with a 6 s fixation cross, which was followed by a transient sensory stimulus. At 10 s after the stimulus, participants were asked to move a slide to rate the perceived intensity of the stimulus on the 0–10 NRS (0, no sensation; 10, the strongest sensation imaginable for each sensory modality) shown on the screen within 5 s. The intertrial interval was 1–2 s. Stimuli were presented using E-Prime v.2.0 (Psychology Software Tools).

Sensory stimulation. A pilot behavioural experiment determined the intensities of sensory stimulation to ensure that the perceived ratings of low- and high-intensity stimuli for each sensory modality were approximately 4 and 7 out of 10, respectively. However, since painful laser stimuli of 4.0 J were unbearable for some participants, we divided all participants into two groups, that is, high and low pain sensitivity participants. High pain sensitivity participants (n = 187) were those who rated 4.0 J laser stimuli >8 out of 10. All remaining participants who rated the 4.0 J stimuli ≤8 out of 10 were assigned to the low pain sensitivity group (n = 212). Two stimulus energies (3.0 and 3.5 J) were applied to participants with high pain sensitivity, while the other two energies (3.5 and 4.0 J) were applied to participants with low pain sensitivity.

Painful stimuli were transient radiant heat pulses (wavelength, 1.34 µm; pulse duration, 4 ms) generated by an infrared neodymium yttrium aluminium perovskite (Nd: YAP) laser (Electronical Engineering). An optic fibre transmitted the laser beam and its diameter was set at ~7 mm. Laser pulses were delivered to a predefined square (5 × 5 cm^2) on the left-hand dorsum. After each stimulus, the laser beam was displaced by ~1 cm in a random direction to avoid nociceptor fatigue or sensitization.

Electrotactile stimuli were constant current square-wave electrical pulses (duration, 1 ms; model DS7A, Digitimer) delivered through a pair of skin electrodes (1 cm interelectrode distance) placed on the left wrist over the superficial radial nerve. The same two stimulus intensities (2.0 and 4.0 mA) were applied to all participants. Auditory stimuli were brief pure tones (frequency, 800 Hz; duration, 50 ms; 5 ms rise and fall time) delivered through a headphone. The same two stimulus intensities (76 and 88 dB SPL) were used for all participants. Visual stimuli were brief flashes of a grey round disk in a black background (duration, 100 ms) on a computer screen. The stimulus intensities were adjusted using the greyscale of the round disk, which corresponded to RGB values of (100, 100, 100) and (200, 200, 200), respectively.

fMRI GLM and conjunction analyses. Single-subject task fMRI data, including functional runs from two blocks, were analysed using a GLM approach to model each stimulus type (pain (P), touch (T), vision (V) and audition (A)) and rating scale as events. Regressors representing the experimental paradigm were then modelled by convolving boxcar functions for each regressor with a canonical haemodynamic response function. After model estimation, we defined contrasts to identify brain responses to different modalities of sensory stimulation using a random-effects analysis with a one-sample t-test. The significance threshold was set as $P < 0.001$ at the voxel level and $P_{FDR} < 0.05$ at the cluster level (false discovery rate (FDR) correction for multiple comparisons) in the whole-brain exploratory analyses. Note that we used two-sided tests whenever applicable.

After obtaining the statistical maps of four stimulus types (P, T, V and A), we aimed to identify somatosensory-preferential and pain-preferential thalamic responses by thresholding t values of the four maps in the thalamus as follows: somatosensory preferential: $P > 3.1$ and $T > 3.1$ and $V \leq 3.1$ and $A \leq 3.1$; pain preferential: $P > 3.1$ and $T \leq 3.1$ and $V \leq 3.1$ and $A \leq 3.1$ (t values > 3.1 corresponds to $P < 0.001$). After identifying the conjunction regions that pass the statistical thresholds, we extracted the normalized BOLD time series in the identified regions from −4 to 10 s relative to the stimulus onset for each stimulus type.

MVPA for fMRI. We constructed SVM-based binary classifiers to discriminate four modalities of stimuli within each participant. For each modality, the normalized BOLD fMRI signals (the second volume after each stimulus onset) in the thalamus were used as features, yielding N pattern vectors per modality (N = 20 trials in the present study). We used a linear SVM classifier (LIBSVM toolbox)[43], with a leave-one-pair-out cross-validation approach, to train the SVM classifier to pairwise decode any two modalities. Specifically, for each participant and pair of modalities (for example, low pain versus low touch; we did not perform classification across different intensities, for example, high pain versus low touch, to eliminate the effects of stimulus intensity), $N - 1$ pattern vectors for each modality consisted of the training set and the remaining pattern vector was used as the test set. This procedure was repeated N times, with each subsample being the test set once. To avoid a potential bias of training-test splits, the cross-validation was performed ten times with random reassignment of the data to training and test sets. The performance of the classifier to distinguish two modalities was evaluated for each participant.

To identify neural patterns underlying the classifications of different sensory modalities, we first transformed the within-participant pattern vectors of classification weights to 'activation patterns' using the method described in previous studies[44,45]. This procedure was performed since the predictive brain regions could be related to sensory modality as well as suppressing the noise in the data[45]. We then evaluate the consistency of within-participant neural patterns in discriminating different sensory modalities by performing one-sample t-tests against

zero across participants. A thresholded map ($P_{FDR} < 0.05$) was used to show the consistent discriminative effect of each paired modality (for example, pain versus touch). To identify a pain-preferential neural pattern, we isolated the conjunct part of three thresholded maps: pain versus touch, pain versus vision and pain versus audition. That is, the neural pattern that could discriminate between pain and the other three modalities.

In addition to discriminating different modalities, we also performed SVM classification within each modality to discriminate between low and high intensities (for example, high and low pain). The procedures and approaches were identical to what we described above.

PPI analysis. We used the identified pain-preferential MD and somatosensory-preferential VPL as seeds to perform the seed-to-voxel PPI analysis to study the thalamocortical functional connectivity when participants experienced different modalities of sensory stimulation[46,47]. For each participant, PPI effects were estimated for different sensory modalities. Individual PPI values for each seed were then compared between different modalities (for example, PPI_{pain} versus PPI_{touch}) using paired-sample *t*-tests. The thresholded statistical maps ($P_{FDR} < 0.05$) were used to show significantly different thalamocortical functional connectivity when experiencing stimuli of different sensory modalities.

Rating matching procedure. Subjective intensity ratings are highly correlated with stimulus salience in well-controlled experimental design (for example, when transient stimuli are delivered in isolation). As a result, any difference in perceptual ratings may result in an incompatible salience level between modalities. To control for this possible confounding factor, we adopted a rating matching procedure to equalize intensity ratings between pain and touch, since they (both as submodalities of somatosensation) are more comparable than pain and audition or vision. To rule out the influence of individual differences, we matched pain intensity ratings and electrotactile intensity ratings in a within-individual manner. Specifically, we manually screened participants whose pain intensity ratings and electrotactile intensity ratings were not significantly different, namely the 95% CI of the rating differences contained 0. With this matching criterion, 166 participants were selected. Due to the high correlation between intensity and salience, the salience level of painful stimuli and electrical stimuli in these participants would be comparable.

Study 1.2—thalamic responses after salience-matched stimuli

Experimental procedures. All experimental sessions (calibration session, behavioural session and MRI session) were conducted within a single day and under identical experimental conditions. The 25 participants received transient stimuli from two sensory modalities: painful and electrotactile. The devices and parameters used were identical to the main experiment as we described above. The ascending method of limits (increasing the stimulus energy in steps of 0.25 J or 0.25 mA until the target rating was reported) was used in the calibration session to determine the laser/electrical energies for each individual when they had subjective ratings of 5 and 8, respectively. The energies averaged across three tests were used for the following sessions.

Following the calibration session, participants were presented with painful and electrotactile stimuli, each at two different intensities (high and low). The behavioural experiment consisted of a single block of 40 sensory stimuli, with 10 trials for each stimulus intensity in each sensory modality. The order of stimulus modality and intensity was pseudorandomized. Each trial began with a 2 s fixation cross, followed by a transient sensory stimulus. Participants were asked to orally report the perceived intensity and salience of the stimulus separately on the 0–10 NRS within 4 s after the stimulus and 6 s before the start of the next trial. A rating of 0 represented no sensation or salience, while 10 represented the strongest sensation or highest salience imaginable for each sensory modality. The stimulus salience was explained to participants as 'the ability of the stimulus to capture attention'. The intertrial interval was 7–8 s. The timings and sequence of the experiment are detailed in Supplementary Fig. 6. During the behavioural experiment, electrodermal activity was recorded using a pair of surface round electrodes attached to the medial phalanges of the index and middle fingers of the participant's left hand. The electrodes were connected to Lead108 carbon leads from BIOPAC Systems and the signal was amplified using an MP150 analogue amplifier (BIOPAC Systems). Signals were digitized at a sampling rate of 2,000 Hz using a CED 1401 analogue-to-digital converter (Cambridge Electronic Design).

The fMRI experiment consisted of two blocks, each with 40 sensory stimuli (10 stimuli for each modality and intensity) delivered in the MRI scanner, using the same stimulus intensities as in the behavioural experiment. The order of stimulus modality and intensity was pseudorandomized in each block. Each trial began with a 6 s fixation cross, followed by a transient sensory stimulus. Participants were asked to rate the perceived intensity and salience of the stimulus separately using the 0–10 NRS shown on the screen within 5 s after the stimulus and the intertrial interval was 1–2 s (Supplementary Fig. 6). Stimuli were presented using E-Prime 2.0 (Psychology Software Tools).

SCR analysis. SCR analysis was performed using the Ledalab toolbox for MATLAB[48]. To facilitate subsequent processing, the data were downsampled to 500 Hz. Subsequently, continuous decomposition analysis was used to decompose the raw data into phasic and tonic components. The phasic SCR was computed on the basis of the phasic component and the maximum value of phasic activity was determined for each experimental stimulus within the response window (1–4 s after stimulus onset).

Study 2—pain-preferential MD spatiotemporal neural dynamics

Experimental procedures. The 220 participants who participated in study 1 received different modalities of sensory stimulation during EEG recording. The EEG experiment consisted of three blocks (40 sensory stimuli in each block). The structure of each trial was similar to the fMRI experiment, except the timings were adjusted. Each trial began with a 3 s fixation cross, followed by a transient sensory stimulus. At 3 s after the stimulus, participants were asked to verbally rate the perceived intensity of the stimulus using the 0–10 NRS within 5 s. The intertrial interval was 1–3 s. Stimuli were presented using E-Prime 2.0 (Psychology Software Tools).

Sensory stimulation. Sensory stimuli used in study 2 were identical to those in study 1.1.

Time-resolved MVPA for EEG. For each time point in the peristimulus EEG signal, from −500 to 1,000 ms (1 ms resolution) with respect to stimulus onset, we constructed pattern vectors by concatenating the 64 EEG electrode measures into 64-dimensional vectors as features. We used a leave-one-pair-out cross-validation approach to train and test the SVM classifier to discriminate between any pair of sensory modalities. The classification procedure was similar to the fMRI MVPA. The resultant classification accuracies were stored in a symmetric 4 × 4 decoding matrix (each cell indicated the accuracy that the classifier distinguished between two modalities; accuracies across different intensities were averaged), with rows and columns indexed by the modalities classified. This procedure was repeated for each time point and pair of modalities, yielding one 4 × 4 matrix of decoding accuracies for every time point.

EEG–fMRI fusion analysis. The technical details of EEG–fMRI fusion were comprehensively described in a recent paper[18]. This method could link multivariate response patterns of the human brain recorded

using fMRI and EEG based on the representational similarity. In this study, the procedures were shown in Fig. 5a. We built a classification assignment, including 12 binary tasks to discriminate pain and three modalities (high/low pain versus high/low touch/vision/audition, at within-participant level), to link response patterns in datasets sampled using two different recording techniques. For fMRI, we used voxel-wise BOLD signals in the MD as features, resulting in a vector of classification accuracies (fMRI dissimilarity vector) for each participant. For EEG, we used 64-channel EEG data at each time point as features, resulting in a vector of classification accuracies (EEG dissimilarity vector) for each time point and each participant. We then evaluated the extent of similar representations between participant-level fMRI in the MD and EEG by computing Spearman's rank-order correlations between fMRI dissimilarity vector and EEG dissimilarity vectors (separately for each time point).

Study 3—pain-preferential thalamocortical dynamics in rats

Experimental procedures. Details of the surgical procedure are given in our previous publications[49,50]. Animal experiments included two blocks. The painful and electrotactile stimuli of two intensities (high and low) were applied to the rat's forepaw and there were 30/40 trials for each stimulus intensity. The painful stimuli were similar to the human study but a small laser spot (diameter, ~5 mm) was used, with low- and high-intensity laser stimuli set to 2.5 and 3.5 J, respectively. The electrotactile stimuli were constant current square-wave electrical pulses (duration, 1 ms), with low- and high-intensity electrical stimuli adjusted at 500 μA and 1 mA, respectively. During the signal recording session, a rat was placed into a plastic chamber ($30 \times 30 \times 40$ cm^3) and allowed to move freely. The chamber floor was a stainless steel mesh plate with regular holes with a diameter of 5 mm to facilitate stimulation. When the animal was spontaneously motionless, stimulation was delivered on the plantar surface of the left or right forepaw via holes in the chamber floor. To avoid potential sensory interference, we always performed the electrotactile block first and let rats rest for about 30 min before the painful block. The order of stimulation site and intensity was pseudorandomized in each block. The interstimulus intervals of electrotactile and painful stimuli were >20 and >40 s, respectively. After the experiment, the rats were perfused, their brain tissues were sectioned consecutively and the electrode position was verified by digital microscope photography.

Data analysis. Since the MUA is considered to be a reliable representative of the average spiking of small neuronal populations near the microelectrode tip[51], the MUA was grouped and averaged to represent the neuronal responses in each brain region (ACC, S1, MD and VPL). The raw data were initially segmented into a 1,500 ms time window (−500 to 1,000 ms to stimulus onset). A shorter time window (−200–600 ms) was used to display the spike firing responses for both modalities. To compare the modulation of spike firing rates by painful and electrotactile stimuli, the trial averaged spike firing rate of MUA was smoothed by a Gaussian kernel with 10 ms using the psth.m function of the Chronux toolbox[52] and then normalized by subtracting the spontaneous activity of prestimulus interval. For painful and electrotactile stimuli, we extracted the mean firing rates within 200 and 100 ms after stimulus onset for each brain region (VPL, S1, MD and ACC) and each stimulus intensity (low and high), respectively.

To assess the relationship of spiking activities sampled at four brain regions, we calculated the SSC using the cohgrampb function of the Chronux toolbox[52]. This method is suitable for computing the two binned point processes of spike activity and calculating a multitaper time–frequency coherence. For the multitaper estimate, the time-bandwidth product was set as three and five tapers were used. Specifically, the Fourier transforms of the two signals (x, binned point process data of one brain region; y, binned point process data of another brain region) were used to calculate multitaper estimates across spectra $S_{xy}(f)$. Time–frequency distributions of SSC were calculated using a 100 ms sliding window, with a step of 10 ms. For each frequency and trial, SSC was normalized by subtracting the mean of the prestimulus interval. Finally, according to the distribution of the time–frequency coherogram, the mean coherence value extracted within the time–frequency region showed apparent coherence (0–200 ms, 1–40 Hz for painful stimuli; 0–100 ms, 1–40 Hz for electrotactile stimuli) for each stimulus intensity (low and high) and pathway (VPL–S1 and MD–ACC).

Statistical considerations

All statistical tests were two-sided unless otherwise stated explicitly. When statistical assumptions were unlikely to be met, permutation tests and bootstrap tests were adopted.

Permutation test. Nonparametric permutation tests were used for cluster-size inference of (1) EEG decoding time series and (2) EEG–fMRI time-resolved similarity indices[53]. The details are described in previous studies[54,55]. In this study, the null hypotheses were (1) the EEG decoding time series was equal to 50% chance level; (2) the correlation of the EEG decoding matrices and fMRI decoding matrix was equal to 0. We permuted the labels (for example, pain or touch) of the EEG data, which was equivalent to a sign-permutation test that randomly multiplied the EEG decoding accuracies/ EEG–fMRI decoding correlations with +1 or −1. We used 1,000 permutations, 0.001 cluster-defining threshold and 0.05 cluster threshold to identify the time windows during which (1) EEG data could significantly discriminate between pain and other three modalities and (2) fMRI BOLD responses in the MD and EEG responses were significantly correlated when distinguishing pain and other three modalities.

Bootstrap test. Bootstrap tests were used to evaluate the latency differences in the EEG decoding time series. We created 1,000 bootstrapped samples by sampling the participants with replacement. For each bootstrap sample, we repeated the exact data analysis as the original data, resulting in bootstrap estimates of onset latencies and thus determining their 95% CI.

Reporting summary

Further information on research design is available in the Nature Portfolio Reporting Summary linked to this article.

Data availability

Individual fMRI, EEG and rodent electrophysiological data are available at ScienceDB (https://doi.org/10.57760/sciencedb.psych.00120).

Code availability

MRI and EEG data analyses were based on standard procedures and codes in SPM and EEGLAB. The machine learning based analyses were based on the codes in LIBSVM. Customized codes for EEG-fMRI fusion can be requested from the corresponding authors.

References

1. Raja, S. N. et al. The revised International Association for the Study of Pain definition of pain: concepts, challenges and compromises. *Pain* **161**, 1976–1982 (2020).
2. Wager, T. D. et al. An fMRI-based neurologic signature of physical pain. *N. Engl. J. Med.* **368**, 1388–1397 (2013).
3. Tu, Y. et al. Alpha and gamma oscillation amplitudes synergistically predict the perception of forthcoming nociceptive stimuli. *Hum. Brain Mapp.* **37**, 501–514 (2016).
4. Legrain, V., Iannetti, G., Plaghki, L. & Mouraux, A. The pain matrix reloaded: a salience detection system for the body. *Prog. Neurobiol.* **93**, 111–124 (2011).

5. Liang, M., Su, Q., Mouraux, A. & Iannetti, G. D. Spatial patterns of brain activity preferentially reflecting transient pain and stimulus intensity. *Cereb. Cortex* **29**, 2211–2227 (2019).
6. Ghazanfar, A. A. & Schroeder, C. E. Is neocortex essentially multisensory? *Trends Cogn. Sci.* **10**, 278–285 (2006).
7. Liang, M., Mouraux, A., Hu, L. & Iannetti, G. D. Primary sensory cortices contain distinguishable spatial patterns of activity for each sense. *Nat. Commun.* **4**, 1979 (2013).
8. Kayser, C. The multisensory nature of unisensory cortices: a puzzle continued. *Neuron* **67**, 178–180 (2010).
9. Mouraux, A., Diukova, A., Lee, M. C., Wise, R. G. & Iannetti, G. D. A multisensory investigation of the functional significance of the 'pain matrix'. *Neuroimage* **54**, 2237–2249 (2011).
10. Su, Q. et al. Brain regions preferentially responding to transient and iso-intense painful or tactile stimuli. *Neuroimage* **192**, 52–65 (2019).
11. Zhang, X. et al. A multisensory fMRI investigation of nociceptive-preferential cortical regions and responses. *Front. Neurosci.* **15**, 420 (2021).
12. Tang, J. et al. Brain gene expression pattern correlated with the differential brain activation by pain and touch in humans. *Cereb. Cortex* **31**, 3506–3521 (2021).
13. Auvray, M., Myin, E. & Spence, C. The sensory-discriminative and affective-motivational aspects of pain. *Neurosci. Biobehav. Rev.* **34**, 214–223 (2010).
14. Coghill, R. C. The distributed nociceptive system: a framework for understanding pain. *Trends Neurosci.* **43**, 780–794 (2020).
15. Kulkarni, B. et al. Attention to pain localization and unpleasantness discriminates the functions of the medial and lateral pain systems. *Eur. J. Neurosci.* **21**, 3133–3142 (2005).
16. Najdenovska, E. et al. In-vivo probabilistic atlas of human thalamic nuclei based on diffusion-weighted magnetic resonance imaging. *Sci. Data* **5**, 180270 (2018).
17. Horing, B., Sprenger, C. & Büchel, C. The parietal operculum preferentially encodes heat pain and not salience. *PLoS Biol.* **17**, e3000205 (2019).
18. Cichy, R. M. & Oliva, A. A M/EEG-fMRI fusion primer: resolving human brain responses in space and time. *Neuron* **107**, 772–781 (2020).
19. Mouraux, A. & Iannetti, G. D. The search for pain biomarkers in the human brain. *Brain* **141**, 3290–3307 (2018).
20. Borsook, D., Edwards, R., Elman, I., Becerra, L. & Levine, J. Pain and analgesia: the value of salience circuits. *Prog. Neurobiol.* **104**, 93–105 (2013).
21. Apkarian, A. V., Bushnell, M. C., Treede, R. D. & Zubieta, J. K. Human brain mechanisms of pain perception and regulation in health and disease. *Eur. J. Pain* **9**, 463–484 (2005).
22. Iannetti, G. D., Hughes, N. P., Lee, M. C. & Mouraux, A. Determinants of laser-evoked EEG responses: pain perception or stimulus saliency? *J. Neurophysiol.* **100**, 815–828 (2008).
23. Seminowicz, D. A. & Davis, K. D. Interactions of pain intensity and cognitive load: the brain stays on task. *Cereb. Cortex* **17**, 1412–1422 (2007).
24. Wiech, K., Ploner, M. & Tracey, I. Neurocognitive aspects of pain perception. *Trends Cogn. Sci.* **12**, 306–313 (2008).
25. Salomons, T. V., Iannetti, G. D., Liang, M. & Wood, J. N. The 'pain matrix' in pain-free individuals. *JAMA Neurol.* **73**, 755–756 (2016).
26. Segerdahl, A. R., Mezue, M., Okell, T. W., Farrar, J. T. & Tracey, I. The dorsal posterior insula subserves a fundamental role in human pain. *Nat. Neurosci.* **18**, 499–500 (2015).
27. Lieberman, M. D. & Eisenberger, N. I. The dorsal anterior cingulate cortex is selective for pain: results from large-scale reverse inference. *Proc. Natl Acad. Sci. USA* **112**, 15250–15255 (2015).
28. Downar, J., Crawley, A. P., Mikulis, D. J. & Davis, K. D. A multimodal cortical network for the detection of changes in the sensory environment. *Nat. Neurosci.* **3**, 277–283 (2000).
29. Heeger, D. J. & Ress, D. What does fMRI tell us about neuronal activity? *Nat. Rev. Neurosci.* **3**, 142–151 (2002).
30. Tu, Y. et al. Distinct thalamocortical network dynamics are associated with the pathophysiology of chronic low back pain. *Nat. Commun.* **11**, 3948 (2020).
31. Woolf, C. J. & Mannion, R. J. Neuropathic pain: aetiology, symptoms, mechanisms and management. *Lancet* **353**, 1959–1964 (1999).
32. Colloca, L. et al. Neuropathic pain. *Nat. Rev. Dis. Prim.* **3**, 17002 (2017).
33. Zhou, L. et al. A modality-specific dysfunction of pain processing in schizophrenia. *Hum. Brain Mapp.* **41**, 1738–1753 (2020).
34. Grossman, N. et al. Noninvasive deep brain stimulation via temporally interfering electric fields. *Cell* **169**, 1029–1041 (2017).
35. Todd, N., McDannold, N. & Borsook, D. Targeted manipulation of pain neural networks: the potential of focused ultrasound for treatment of chronic pain. *Neurosci. Biobehav. Rev.* **115**, 238–250 (2020).
36. Paxinos, G. & Watson, C. *The Rat Brain in Stereotaxic Coordinates* 6th edn (Academic Press, 2006).
37. Yue, L., Iannetti, G. D. & Hu, L. The neural origin of nociceptive-induced gamma-band oscillations. *J. Neurosci.* **40**, 3478–3490 (2020).
38. Ashburner, J. & Friston, K. Unified segmentation. *Neuroimage* **26**, 839–851 (2005).
39. Ciric, R. et al. Benchmarking of participant-level confound regression strategies for the control of motion artifact in studies of functional connectivity. *Neuroimage* **154**, 174–187 (2017).
40. Delorme, A. & Makeig, S. EEGLAB: an open source toolbox for analysis of single-trial EEG dynamics including independent component analysis. *J. Neurosci. Methods* **134**, 9–21 (2004).
41. Hazan, L., Zugaro, M. & Buzsáki, G. Klusters, NeuroScope, NDManager: a free software suite for neurophysiological data processing and visualization. *J. Neurosci. Methods* **155**, 207–216 (2006).
42. Rossant, C. et al. Spike sorting for large, dense electrode arrays. *Nat. Neurosci.* **19**, 634–641 (2016).
43. Chang, C. & Lin, C. LIBSVM: a library for support vector machines. *ACM Trans. Intell. Syst. Technol.* **2**, 27 (2011).
44. Zhou, F. et al. A distributed fMRI-based signature for the subjective experience of fear. *Nat. Commun.* **12**, 6643 (2021).
45. Haufe, S. et al. On the interpretation of weight vectors of linear models in multivariate neuroimaging. *Neuroimage* **87**, 96–110 (2014).
46. Friston, K. J. et al. Psychophysiological and modulatory interactions in neuroimaging. *Neuroimage* **6**, 218–229 (1997).
47. Di, X. & Biswal, B. Toward task connectomics: examining whole-brain task modulated connectivity in different task domains. *Cereb. Cortex* **29**, 1572–1583 (2019).
48. Benedek, M. & Kaernbach, C. A continuous measure of phasic electrodermal activity. *J. Neurosci. Methods* **190**, 80–91 (2010).
49. Hu, L. et al. Was it a pain or a sound? Across-species variability in sensory sensitivity. *Pain* **156**, 2449–2457 (2015).
50. Yue, L., Zhang, F., Lu, X., Wan, Y. & Hu, L. Simultaneous recordings of cortical local field potentials and electrocorticograms in response to nociceptive laser stimuli from freely moving rats. *J. Vis. Exp.* **2019**, e58686 (2019).
51. Buzsáki, G. Large-scale recording of neuronal ensembles. *Nat. Neurosci.* **7**, 446–451 (2004).
52. Bokil, H. andrews, P., Kulkarni, J. E., Mehta, S. & Mitra, P. P. Chronux: a platform for analyzing neural signals. *J. Neurosci. Methods* **192**, 146–151 (2010).
53. Maris, E. & Oostenveld, R. Nonparametric statistical testing of EEG- and MEG-data. *J. Neurosci. Methods* **164**, 177–190 (2007).

54. Tu, Y. et al. How expectations of pain elicited by consciously and unconsciously perceived cues unfold over time. *Neuroimage* **235**, 117985 (2021).
55. Cichy, R. M., Pantazis, D. & Oliva, A. Resolving human object recognition in space and time. *Nat. Neurosci.* **17**, 455–462 (2014).

Acknowledgements

Y.T. is supported by STI2030-Major Projects by the Ministry of Science and Technology of China (grant no. 2022ZD0206400), National Natural Science Foundation of China (grant nos. 32171078 and 32322035), Scientific Foundation of the Institute of Psychology, Chinese Academy of Sciences (grant nos. E0CX52 and E2CX4015) and Young Elite Scientist Sponsorship Program by the China Association for Science and Technology (grant no. E1KX0210). L.H. is supported by National Natural Science Foundation of China (grant no. 32071061) and Beijing Natural Science Foundation (grant no. JQ22018). The funders had no role in study design, data collection and analysis, decision to publish or preparation of the manuscript.

Author contributions

This work was conceptualized by Y.T. and L.H. who also developed the methodology, undertook project administration and supervision and acquired funding. Investigation was undertaken by Y.T., H.Z., Z.L., Y.B., L.Y. and L.H. Visualization was by Y.T. and Z.L. The original draft was written by Y.T., with review and editing by Y.T., L.Z. and L.H.

Competing interests

The authors declare no competing interests.

Additional information

Supplementary information The online version contains supplementary material available at https://doi.org/10.1038/s41562-023-01714-6.

Correspondence and requests for materials should be addressed to Yiheng Tu or Li Hu.

Peer review information *Nature Human Behaviour* thanks Ulrike Bingel, Giulia Liberati and Yuan B. Peng for their contribution to the peer review of this work. Peer reviewer reports are available. Peer reviewer reports are available.

nature portfolio

Corresponding author(s): Yiheng Tu, Li Hu

Last updated by author(s): Aug 24, 2023

Reporting Summary

Nature Portfolio wishes to improve the reproducibility of the work that we publish. This form provides structure for consistency and transparency in reporting. For further information on Nature Portfolio policies, see our Editorial Policies and the Editorial Policy Checklist.

Statistics

For all statistical analyses, confirm that the following items are present in the figure legend, table legend, main text, or Methods section.

n/a	Confirmed	
☐	☒	The exact sample size (*n*) for each experimental group/condition, given as a discrete number and unit of measurement
☐	☒	A statement on whether measurements were taken from distinct samples or whether the same sample was measured repeatedly
☐	☒	The statistical test(s) used AND whether they are one- or two-sided *Only common tests should be described solely by name; describe more complex techniques in the Methods section.*
☒	☐	A description of all covariates tested
☐	☒	A description of any assumptions or corrections, such as tests of normality and adjustment for multiple comparisons
☐	☒	A full description of the statistical parameters including central tendency (e.g. means) or other basic estimates (e.g. regression coefficient) AND variation (e.g. standard deviation) or associated estimates of uncertainty (e.g. confidence intervals)
☐	☒	For null hypothesis testing, the test statistic (e.g. *F*, *t*, *r*) with confidence intervals, effect sizes, degrees of freedom and *P* value noted *Give P values as exact values whenever suitable.*
☒	☐	For Bayesian analysis, information on the choice of priors and Markov chain Monte Carlo settings
☒	☐	For hierarchical and complex designs, identification of the appropriate level for tests and full reporting of outcomes
☐	☒	Estimates of effect sizes (e.g. Cohen's *d*, Pearson's *r*), indicating how they were calculated

Our web collection on statistics for biologists contains articles on many of the points above.

Software and code

Policy information about availability of computer code

Data collection	Data were collected using E-Prime (ver. 2.0, PST Inc.)
Data analysis	FMRI data were analyzed using SPM12 (https://www.fil.ion.ucl.ac.uk/spm/software/spm12/) and custom Matlab code (ver. R2020a; Mathwork). EEG data were analyzed using EEGLAB (ver. 2019_1; https://sccn.ucsd.edu/eeglab/index.php) and custom Matlab code. SVM classification was conducted using the LIBSVM toolbox (ver. 3.22; https://www.csie.ntu.edu.tw/~cjlin/libsvm/). Rat electrophysiology data were analyzed using NDManager (ver. 2.0.0; https://github.com/neurosuite/ndmanager), KlustaKwik (ver. 3.0.2; https://github.com/klusta-team/klustakwik), Chronux (ver. 2.12; http://chronux.org/), and custom Matlab code.

For manuscripts utilizing custom algorithms or software that are central to the research but not yet described in published literature, software must be made available to editors and reviewers. We strongly encourage code deposition in a community repository (e.g. GitHub). See the Nature Portfolio guidelines for submitting code & software for further information.

Data

Policy information about availability of data

All manuscripts must include a data availability statement. This statement should provide the following information, where applicable:

- Accession codes, unique identifiers, or web links for publicly available datasets
- A description of any restrictions on data availability
- For clinical datasets or third party data, please ensure that the statement adheres to our policy

Source data are publicly available at ScienceDB (https://doi.org/10.57760/sciencedb.psych.00120).

Human research participants

Policy information about studies involving human research participants and Sex and Gender in Research.

Reporting on sex and gender	Findings apply to males and females, which was determined based on self-reporting. We did not purposefully control the male-to-female ratio. Study 1.1 included 160 males and 237 females (two participants did not provide sex information); Study 1.2 included 3 males and 22 females; Study 2 included 92 males and 128 females.
Population characteristics	Study 1 included 399 healthy participants (160 males; age 21.3±3.8 years, mean±SD; two participants did not provide demographic information) and 25 healthy participants (3 males; age 22.3±2.9 years) who were pain-free and had no history of chronic pain and neuropsychiatric disorders. Study 2 included 220 healthy participants (92 males; age 20.8±2.3 years).
Recruitment	Participants in Studies 1 and 2 were recruited via advertisements posted on social media like WeChat. The recruitment could have been biased towards younger, educated population as the majority of the participants were college students. In addition, there could be a sampling bias related to the unwillingness to participate in pain research.
Ethics oversight	Studies 1 and 2: the Ethical Committee at the Institute of Psychology, Chinese Academy of Sciences.

Note that full information on the approval of the study protocol must also be provided in the manuscript.

Field-specific reporting

Please select the one below that is the best fit for your research. If you are not sure, read the appropriate sections before making your selection.

☒ Life sciences ☐ Behavioural & social sciences ☐ Ecological, evolutionary & environmental sciences

For a reference copy of the document with all sections, see nature.com/documents/nr-reporting-summary-flat.pdf

Life sciences study design

All studies must disclose on these points even when the disclosure is negative.

Sample size	No sample size calculation was performed. Studies 1 and 2 included hundreds of subjects, making it statistically powerful enough to detect small effects. The data collection for these datasets lasted for two years and we collected as many participants as possible, resulting in the specific sample sizes. The sample sizes in Study 3 (N = 9) were based on previous studies with similar design and goals (e.g., Tan et al. 2019, https://doi.org/10.1038/s41467-019-08873-z; Yue et al., 2020, https://doi.org/10.1523/JNEUROSCI.0255-20.2020).
Data exclusions	No data were excluded.
Replication	No direct replication was conducted, but Studies 3 (rat electrophysiology data) successfully validated findings from Studies 1 and 2 (healthy participant data).
Randomization	Studies 1, 2, and 3 needed no randomization since all subjects underwent all (within-subjects) experimental conditions.
Blinding	Blinding was not relevant. We didn't test the efficacy of any interventions, but only delivered stimuli of different sensory modalities to participants and asked them to report their subjective perception. The purpose of these datasets (i.e., investigating neural underpinnings of sensory information processing) were also transparent to participants.

Behavioural & social sciences study design

All studies must disclose on these points even when the disclosure is negative.

Study description	
Research sample	
Sampling strategy	
Data collection	
Timing	
Data exclusions	
Non-participation	
Randomization	

Ecological, evolutionary & environmental sciences study design

All studies must disclose on these points even when the disclosure is negative.

Study description	
Research sample	
Sampling strategy	
Data collection	
Timing and spatial scale	
Data exclusions	
Reproducibility	
Randomization	
Blinding	

Did the study involve field work? ☐ Yes ☐ No

Field work, collection and transport

Field conditions	
Location	
Access & import/export	
Disturbance	

Reporting for specific materials, systems and methods

We require information from authors about some types of materials, experimental systems and methods used in many studies. Here, indicate whether each material, system or method listed is relevant to your study. If you are not sure if a list item applies to your research, read the appropriate section before selecting a response.

Materials & experimental systems

n/a	Involved in the study
☒	☐ Antibodies
☒	☐ Eukaryotic cell lines
☒	☐ Palaeontology and archaeology
☐	☒ Animals and other organisms
☒	☐ Clinical data
☒	☐ Dual use research of concern

Methods

n/a	Involved in the study
☒	☐ ChIP-seq
☒	☐ Flow cytometry
☐	☒ MRI-based neuroimaging

Antibodies

Antibodies used

Validation

Eukaryotic cell lines

Policy information about cell lines and Sex and Gender in Research

Cell line source(s)

Authentication

Mycoplasma contamination

Commonly misidentified lines
(See ICLAC register)

Palaeontology and Archaeology

Specimen provenance

Specimen deposition

Dating methods

☐ Tick this box to confirm that the raw and calibrated dates are available in the paper or in Supplementary Information.

Ethics oversight

Note that full information on the approval of the study protocol must also be provided in the manuscript.

Animals and other research organisms

Policy information about studies involving animals; ARRIVE guidelines recommended for reporting animal research, and Sex and Gender in Research

Laboratory animals	Nine adult male Sprague-Dawley rats (weighing 350 to 450 g).
Wild animals	The study did not involve wild animals
Reporting on sex	In this study, only male rats were included. The estrus or menstrual period of female rats is difficult to control and can complicate data analysis. In addition, it is much easier to compare our findings with previous ones, since most previous studies with similar goals use only male rats.
Field-collected samples	The study did not involve samples collected from the field.
Ethics oversight	The Animal Care and Use Committee and Ethical Committee of the Institute of Psychology, Chinese Academy of Sciences

Note that full information on the approval of the study protocol must also be provided in the manuscript.

Clinical data

Policy information about clinical studies

All manuscripts should comply with the ICMJE guidelines for publication of clinical research and a completed CONSORT checklist must be included with all submissions.

Clinical trial registration	/
Study protocol	/
Data collection	/
Outcomes	/

Dual use research of concern

Policy information about dual use research of concern

Hazards

Could the accidental, deliberate or reckless misuse of agents or technologies generated in the work, or the application of information presented in the manuscript, pose a threat to:

No	Yes	
☐	☐	Public health
☐	☐	National security
☐	☐	Crops and/or livestock
☐	☐	Ecosystems
☐	☐	Any other significant area

Experiments of concern

Does the work involve any of these experiments of concern:

No	Yes	
☐	☐	Demonstrate how to render a vaccine ineffective
☐	☐	Confer resistance to therapeutically useful antibiotics or antiviral agents
☐	☐	Enhance the virulence of a pathogen or render a nonpathogen virulent
☐	☐	Increase transmissibility of a pathogen
☐	☐	Alter the host range of a pathogen
☐	☐	Enable evasion of diagnostic/detection modalities
☐	☐	Enable the weaponization of a biological agent or toxin
☐	☐	Any other potentially harmful combination of experiments and agents

ChIP-seq

Data deposition

☐ Confirm that both raw and final processed data have been deposited in a public database such as GEO.

☐ Confirm that you have deposited or provided access to graph files (e.g. BED files) for the called peaks.

Data access links *May remain private before publication.*	
Files in database submission	
Genome browser session (e.g. UCSC)	

Methodology

Replicates	
Sequencing depth	

Antibodies	
Peak calling parameters	
Data quality	
Software	

Flow Cytometry

Plots

Confirm that:

☐ The axis labels state the marker and fluorochrome used (e.g. CD4-FITC).

☐ The axis scales are clearly visible. Include numbers along axes only for bottom left plot of group (a 'group' is an analysis of identical markers).

☐ All plots are contour plots with outliers or pseudocolor plots.

☐ A numerical value for number of cells or percentage (with statistics) is provided.

Methodology

Sample preparation	
Instrument	
Software	
Cell population abundance	
Gating strategy	

☐ Tick this box to confirm that a figure exemplifying the gating strategy is provided in the Supplementary Information.

Magnetic resonance imaging

Experimental design

Design type	task; event-related design
Design specifications	Study 1.1: 2 blocks, 40 trials per block, each trial lasting for ~23s (with inter-trial duration of 1~2s). Study 1.2: 2 blocks, 40 trials per block, each trial lasting for ~12s (with inter-trial duration of 1~2s).
Behavioral performance measures	Subjective intensity and salience ratings were collected.

Acquisition

Imaging type(s)	functional, structural
Field strength	3 T
Sequence & imaging parameters	Studies 1 and 2: (1) fMRI was acquired using gradiant echo sequence with TR = 2s, TE = 29ms, field-of-view = 192mm, matrix size = 64 × 64, slice thickness = 3mm, number of slices = 43, slice order = ascending (interleaved), flip angle = 90 degrees; (2) sMRI was acquired using gradiant echo sequence with TR = 6.896ms, TE = 2.99ms, field-of-view = 256mm, matrix size = 64 × 64, slice thickness = 1mm, number of slices = 176, slice order = ascending (interleaved), flip angle = 8 degrees.
Area of acquisition	Whole brain

Diffusion MRI ☐ Used ☒ Not used

Preprocessing

Preprocessing software	Preprocessing was conducted using SPM12 and included: removal of first 5 volumes, slice timing correction, motion correction (6 motion estimates), normalization (MNI152 template), smoothing (Gaussian kernel of 3mm FWHM), and filtering (0.01Hz~0.10Hz).
Normalization	Images were normalized to the MNI template using non-linear transformation.

Normalization template	MNI152 template.
Noise and artifact removal	We regressed out 6 motion estimates and 2 physiological time series (cerebrospinal fluid and the white matter signals) with global signal regression
Volume censoring	Only the first 5 volumes were discarded to allow for signal stabilization.

Statistical modeling & inference

Model type and settings	Mass univariate analysis: We used a GLM approach to model each stimulus type and rating scale as events at the first level analysis. Regressors representing the experimental paradigm were then modeled by convolving boxcar functions for each regressor with a canonical hemodynamic response function. After model estimation, we defined contrasts to identify brain responses to different modalities of sensory stimulation using a random-effects analysis with a one-sample t-test. PPI analysis: We performed the seed-to-voxel PPI analysis to study the thalamocortical functional connectivitye using pain-preferential MD and somatosensory-preferential VPL as seeds. For each participant, PPI effects were estimated for different sensory modalities. Individual PPI values for each seed were then compared between different modalities (e.g., PPIpain vs. PPItouch) using paired-sample t-tests. Multivariate analysis: We constructed linear support vector machine (SVM) based binary classifiers were constructed to discriminate four modalities of stimuli within each participant. For each modality, the normalized BOLD fMRI signals (the 2nd volume after each stimulus onset) in the thalamus were used as features, yielding N pattern vectors per modality (N = 20 trials in the present study). Model performance was assessed using leave-one-pair-out cross validation. RSA: We built a classification assignment, including 12 binary tasks to discriminate pain and other three modalities to link response patterns in datasets sampled using two different recording techniques. For fMRI, we used voxel-wise BOLD signals in the MD as features, resulting in a vector of classification accuracies (i.e., fMRI dissimilarity vector) for each participant. For EEG, we used 64-channel EEG data at each time point as features, resulting in a vector of classification accuracies (i.e., EEG dissimilarity vector) for each time point and each participant. We then evaluated the extent of similar representations between participant-level fMRI in the MD and EEG by computing Spearman's rank-order correlations between fMRI dissimilarity vector and EEG dissimilarity vectors (separately for each time point).
Effect(s) tested	For mass univariate analysis, we tested the effect of sensory stimulations. For PPI, we tested PPI effects for different sensory modalities. For multivariate analysis, we tested whether the classifier was able to classify stimulus types or stimulus intensities. For RSA, we tested the extent of similar representations between participant-level fMRI in the MD and EEG by computing Spearman's rank-order correlations between fMRI dissimilarity vector and EEG dissimilarity vectors (separately for each time point).

Specify type of analysis: ☐ Whole brain ☐ ROI-based ☒ Both

Statistic type for inference (See Eklund et al. 2016)	Cluster-based inference. P<0.001 at the voxel level and pFDR<0.05 at the cluster level.
Correction	In the whole-brain exploratory analyses, the significance threshold was set as p<0.001 at the voxel level and pFDR<0.05 at the cluster level (false discovery rate [FDR] correction for multiple comparisons). In the RSA, nonparametric permutation tests (1000 permutations, 0.001 cluster defining threshold, and 0.05 cluster threshold) were used for cluster-size inference .

Models & analysis

n/a	Involved in the study
☐	☒ Functional and/or effective connectivity
☒	☐ Graph analysis
☐	☒ Multivariate modeling or predictive analysis

Functional and/or effective connectivity	Connectivity was computed using the Psychophysiological interaction (PPI) analysis.
Graph analysis	
Multivariate modeling and predictive analysis	The independent variables are the normalized BOLD fMRI signals (the 2nd volume after each stimulus onset) in the thalamus. A linear SVM classifier was used with leave-one-pair-out cross-validation approach. The performance of the classifier was assessed using the classification accuracy.